ORIGINAL ARTICLE

Large-scale seismic damage scenario assessment of precast buildings after the May 2012 Emilia earthquake

Lucia Praticò[1] · Marco Bovo[2] · Nicola Buratti[1] · Marco Savoia[1]

Abstract

In May 2012, two strong earthquakes hit the northern Italy revealing the significant seismic vulnerability of precast reinforced concrete structures and causing severe damage and many collapses, and high economic losses. After the lesson learnt from these events, more reliable seismic design criteria have been established for the design of new structures and different approaches have been proposed for the seismic assessment of the existing structures. In this context, the paper presents the results of a first application of the PRESSAFE-disp method, recently proposed by the authors, allowing to define the fragility curves of precast RC buildings at various limit states, including collapse. A stock of 91 precast buildings in the industrial area of San Felice sul Panaro (Modena) was selected as a benchmark case study to verify the reliability of the method in assessing seismic damage scenarios. In particular, with reference to the 2012 seismic ground-motion, two large-scale stochastic models are outlined to predict the number of the buildings collapsed in the area. The first one is based on a Monte Carlo simulation which incorporates the evaluation of the uncertainties, while the second one is a direct simplified calculation. Comparative considerations on the outcomes of the two methods for different seismic intensities are discussed, including the directionality effect of the ground-motion. To test the soundness of the simulations, the results of the two methods are compared with the real data collected through in-situ surveys. The procedures proposed here result, on average, in good agreement with the observed damage scenario. It is worth noting that, due to the inherent simplicity of the methods, they could be implemented to perform scenario-based seismic loss assessments to estimate the financial consequences of an earthquake affecting one or more industrial areas, and to drive the decision-making process for the seismic retrofit of existing precast RC buildings.

Keywords Large-scale seismic assessment · Precast buildings · Scenario simulation · Seismic vulnerability

✉ Lucia Praticò
  lucia.pratico3@unibo.it

1   Department of Civil, Chemical, Environmental, and Material Engineering (DICAM), University of Bologna, Viale Risorgimento 2, Bologna, Italy

2   Department of Agricultural and Food Sciences – Agricultural Engineering (DISTAL), University of Bologna, Viale Fanin 48, Bologna, Italy

🖄 Springer

1 Introduction

The seismic risk assessment of buildings is a diversified field of study, in which researchers develop a variety of methods to estimate and classify fragility, vulnerability as well as potential losses caused by earthquakes. Different approaches, both qualitative and quantitative, are available nowadays to define the performances of existing buildings under earthquakes (see the state of the art in Calvi et al. 2006; Silva et al. 2019).

Nevertheless, the research effort on fragility of precast RC structures was very limited until 2012, in comparison to the large number of studies on cast-in-place reinforced concrete or masonry buildings, as mentioned by Casotto et al. (2015). A recent impulse in the research field concerning precast structures arose after the seismic sequence that, in May 2012, hit several productive areas of the Emilia Romagna region in northern Italy, causing severe damage to structures, material stocks, industrial machineries and some human losses. The two mainshocks, identified in many studies as the "Emilia earthquake", were registered on the 20th and 29th May: the second one, with a moment magnitude of 5.9, had an epicenter located at 12 km east of the first one, characterized by a magnitude of 6.1 (see the data catalogued in Rovida et al. 2020 and Rovida et al. 2022). Both mainshocks were followed by a series of minor earthquakes, more than one thousand seismic shocks with magnitude higher than 2.0, and, among these, 29 shocks with a magnitude higher than 4, according to Dolce et al. (2012).

A peculiar aspect of these seismic events is that they hit territories with several production factories (agrifood, mechanics, biomedical, construction, as well as many smaller industries) located in precast concrete buildings not designed against seismic actions. According to the Regional Agency for the Reconstruction (Agenzia Regionale per la Ricostruzione 2018), almost 3000 productive buildings suffered structural damage and the 45 percent of them either suffered severe damage or collapsed.

The surveys conducted in the aftermath of 2012 Emilia earthquake enabled researchers to acquire a series of observations on the weaknesses and structural deficiencies of precast RC buildings (Liberatore et al. 2013; Belleri et al. 2014; Bournas et al. 2014; Magliulo et al. 2014; Minghini et al. 2016; Savoia et al. 2017; Batalha et al. 2019). All these studies agree in concluding that precast RC buildings, when built without seismic details and prescriptions, represent one of the most seismically vulnerable building typologies (Savoia et al. 2012).

As far as the seismic fragility of precast RC buildings is concerned, several recent studies proposed models using either observational damage data (Buratti et al. 2017; Ongaretto et al. 2019; Rossi et al. 2020) or the results of numerical simulations (Casotto et al. 2015; Babic et al. 2016). Fragility models are used in several types of probabilistic analyses, such as loss, damage, and risk assessment (Ramirez and Miranda 2009; FEMA 2018), which can be performed with different levels of detail, spanning from small-scale analyses on single building, to large-scale assessments at regional or national level. The latter is particularly relevant in the Civil Protection framework, such as the development of national plans for the reduction of seismic risk, the prediction of damage scenarios after possible future earthquakes, and the estimation of damage and casualties in the aftermath of an earthquake. To this regard, in the literature there are various examples of seismic assessments at the territorial scale of cast-in-situ RC and masonry buildings in urban areas (see for instance Maio et al. 2015; Lestuzzi et al. 2016; Formisano et al. 2017; Villar-Vega et al. 2017; Anglade et al. 2020; Polese et al. 2020; da Porto et al. 2021). However, as suggested by Belleri et al. (2021), few studies refer to precast RC

buildings in productive areas (Petruzzelli 2016; Demartino et al. 2017; Ercolino et al. 2018a; Rodriguez et al. 2018; Bosio et al. 2020).

In the present paper, a simplified probabilistic large-scale methodology to evaluate the seismic risk of industrial areas is presented. The procedure outlined here is based on the PRESSAFE-disp method described in Bovo et al. (2022) for the definition of fragility curves and provides a framework for estimating the number of collapsed precast buildings due to an earthquake. The methodology has been applied here to the productive area of San Felice sul Panaro, Modena, Italy, for which detailed data on 91 precast buildings were available, together with careful descriptions of the effects of the 2012 earthquake. In the application of the PRESSAFE-disp method, the structural characteristics and materials properties are those of the pre-earthquake condition of the buildings, in order to simulate their seismic behaviour at the time of the seismic shock. Through the analysis of the documents and surveys data available, the pre-earthquake structural features have been established for each building, together with the damage produced by the main seismic event which hit the area on May 29th 2012. In particular, the damage state has been derived from the documentation provided by the owners requesting national funds for the post-earthquake reconstruction.

A Monte Carlo probabilistic simulation has been performed with the purpose of assessing the average number of collapsed buildings for the scenario selected, considering the uncertainties in the evaluation. The results are also compared with those obtained through an alternative direct simplified simulation, neglecting the effects of the uncertainties included in the Monte Carlo method. Finally, the outcomes of the two procedures are compared with the actual damage scenario observed after the 29th May 2012 earthquake, in order to test the reliability and accuracy of the prediction methods. The problem of defining the seismic input in a scenario-based analysis is also discussed. As a main result, it is shown that the adoption of a seismic intensity which includes the directionality effects of the ground-motion is deemed to provide interesting results, since the outcomes of both large-scale simulation methods are in very good agreement, in terms of number of collapses, with the actual data observed in the area.

2 The PRESSAFE-disp method

In the present work, the fragility curves for the precast buildings located in the case-study industrial area were defined using the PRESSAFE-disp (PRecast Existing Structure Seismic Assessment by Fast Evaluation-displacements) method proposed in Bovo et al. (2022). After the 2012 seismic events, the growing interest in the vulnerability of precast RC buildings led to an increasing number of studies focusing on different characteristics of the behavior of this type of structures (Belleri et al. 2014, 2016, 2018; Bovo and Savoia 2018, 2019; Ercolino et al. 2018b), but without a homogeneous approach at the territorial scale. With the aim of providing a uniform approach suitable for large-scale analyses, the PRESSAFE-disp method proposes the fragility curves of different precast building typologies common in the Mediterranean area. The method is based on the calibration of fragility surfaces that define the seismic fragility curve of a frame of a precast RC building a function of its natural period. These surfaces were defined through the following general procedure organized in five phases (Fig. 1):
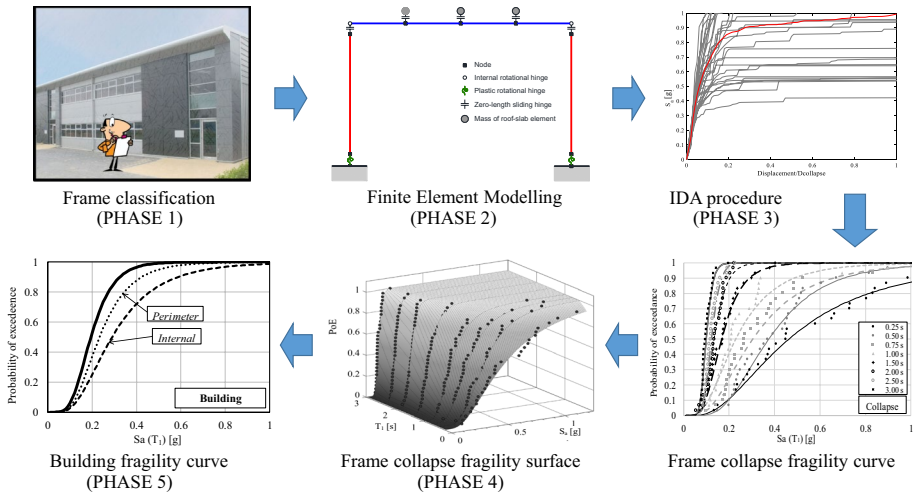
Fig. 1 Flow chart of the PRESSAFE-disp method

1. Classification of the precast frames in categories, by identifying the parameters that mainly influence their seismic response;
2. Non-linear finite element modelling of the frames. Assuming an infinitely flexible roof, perimeter frames and internal frames are studied separately. For each frame, eight different values of the natural period are considered;
3. Incremental dynamic analyses for each frame category and for the various natural periods selected;
4. Calibration of the fragility curves, and thus the fragility surfaces, for each category of internal and perimeter frames. The surfaces express the fragility curve of a frame as a function of its period;
5. Derivation of the fragility curve of the precast RC building by combining the fragility functions of its frames.

The fragility surfaces obtained in phase 4 are used to estimate the fragility of a generic precast RC building in phase 5: given the natural period of perimeter and internal frames, their fragility curves are obtained from the fragility surfaces, and then combined in order to define a fragility curve for the entire building. For the sake of clarity, a description of the main phases of the method is reported in the following subsections, while for further details on the method the reader can refer to Bovo et al. (2022).

2.1 Phase 1: classification of the Italian precast RC buildings

Their characteristic feature is the simplicity of the structural scheme which lacks structural redundancy, consisting of simply-supported beams, roofing elements and cantilever columns. According to Bonfanti et al. (2008), Mandelli et al. (2008), Reluis (2012) and Bellotti et al. (2014), the Italian industrial buildings typically have precast RC floor elements and beams characterized by a limited variety of cross-sections and span lengths, as well as of connection types, because of their strong standardization. Therefore, it is possible to classify them defining few structural categories.

The first step of the PRESSAFE-disp method is the identification and classification of the most representative types of precast structures. Data on these constructions were drawn from databases collecting post-earthquake damage assessment surveys by experts and engineers, after the 2012 Emilia earthquake (Bellotti et al. 2014; Ongaretto et al. 2019). The typical structural layout of one-storey precast industrial buildings is constituted by cantilever columns supporting horizontal precast main beams bearing orthogonal secondary beams (roofing elements). The foundations are usually isolated RC socket foundations. In the PRESSAFE-disp method, the precast buildings were classified according to the four main criteria illustrated in Fig. 2, selected for their significant influence on the seismic behaviour of the frames. The first criterion is based on the value of the yielding moment at the base of columns, for which 4 reference values were selected, indicated with letters from A (the lowest) to D (the highest). The second criterion corresponds to the beam-column connection adopted, associated to three different levels of strength and indicated with letters (L), (M) or (H). The third is the kind of roof slab-to-beam connection, for which two different levels of strength are assumed (i.e. low strength and high strength, labelled L and H, respectively). All these parameters were selected through the analysis of previous studies focused on the capacity of the frame elements and the different connections in precast buildings (Mandelli Contegni et al. 2007; Biondini et al. 2013; Bournas et al. 2013; Magliulo et al. 2015; Belleri et al. 2018).

Considering different combinations of the aforementioned parameters, 24 types of Internal (I) frames and 96 types of Perimeter (P) were considered, for a total of 120 structures. For the perimeter frames, four types of cladding panels were also selected, i.e. masonry infill walls (m), horizontal cladding panels with strong connections (h1) and with weak connections (h2), vertical cladding panels (v).
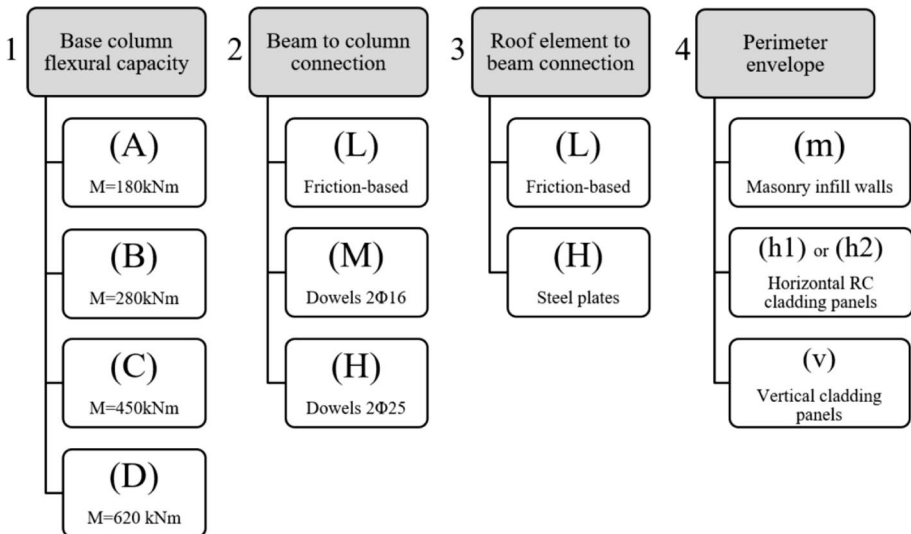

Fig. 2 The four criteria adopted in the PRESSAFE-disp method for the classification of the frames

2.2 Phase 2: non-linear finite element modelling

The non-linear behaviour of the precast columns was modelled by means of plastic hinges at their bases adopting trilinear moment-rotation laws. The non-linear behaviour of both beam-column and roof-beam connections was modelled with zero-length sliding hinges, which are either rigid-plastic in the case of friction-based connections or elastic–plastic in the case of mechanical connectors. Masonry infill walls were modelled with two equivalent diagonal struts between the columns, and cladding panels were modelled as equivalent beam elements connected to beams or to columns, if horizontal or vertical, respectively.

All the constitutive parameters, and the parameters of the connections were defined from experimental tests available in literature (Crisafulli et al. 2000; Asteris et al. 2011; Belleri et al. 2016; Zoubek et al. 2016; Del Monte et al. 2019), and a detailed description of each of them can be found in Bovo et al. (2022).

2.3 Phase 3: incremental dynamic analysis

In order to evaluate the seismic response of the various frames, non-linear Incremental Dynamic Analyses (IDA) were carried out considering both the horizontal and the vertical components of 30 recorded ground-motion accelerograms (see Vamvatsikos and Fragiadakis 2010). For each of the 120 non-linear frames analysed, 8 different values of the natural period (i.e. 0.25 s, 0.5 s, 0.75 s, 1.0 s, 1.5 s, 2.0 s, 2.5 s and 3.0 s) were adopted, to consider the stiffness and mass variability of the frames. In total, 960 different structures were obtained. For each one of them, the collapse condition was defined at the attainment of one of the following conditions:

1. the ultimate chord rotation of columns;
2. the ultimate displacement capacity in the sliding hinges between main beams and columns, defined as either the displacement capacity of mechanical connectors or 10 cm in the case of friction-based connections;
3. the displacement capacity in the sliding hinges between roof slab elements and main beams, defined as either the displacement capacity of mechanical connectors or 5 cm in the case of friction-based connections;

The ground-motion Intensity Measure (IM) considered in the IDAs is the 5%-damped spectral acceleration at the natural period of vibration $S_a(T_1,5\%)$, or S_a in the following, and the Engineering Demand Parameter (EDP) is the maximum horizontal displacement at the roof level.

2.4 Phase 4: definition of the fragility surfaces

For each frame, the results of the IDAs were used to calculate the cumulative fraction of structures reaching a specific damage state (i.e., the collapse) for different IM values, so providing the fragility estimate. The results of the time-history analyses were 28′800 IDA curves, which lead to 960 fragility curves. Each of these curves was then fit by a log-normal cumulative distribution function $F(S_a)$:

$$F(S_a) = \Phi \left[\frac{\ln\left(\frac{S_a}{\mu}\right)}{\sigma} \right] \tag{1}$$

where Φ [·] is the standardized cumulative normal distribution function and μ and σ are the median value and the logarithmic standard deviation of the lognormal distribution. For each frame, the 8 fragility curves (one per natural period of vibration) were then interpolated by a continuous function of S_a and T_1, thus obtaining the 3D fragility surfaces $R(S_a, T_1)$. The analytical expression of the fragility surfaces, providing the probability of exceedance (PoE) for the collapse limit state as a function of S_a and T_1, was obtained by means of a regression model describing the dependency of μ and σ on T_1, i.e.:

$$\text{for } 0 < T_1 \le 2.0 \text{ s} \quad \mu^C(T_1) = a_1 \cdot T_1^2 + a_2 \cdot T_1 + a_3 \tag{2}$$

$$\text{for } 2.0 \text{ s} < T_1 < 3.0 \text{ s} \quad \mu^C(T_1) = \mu^C(2.0) \tag{3}$$

and:

$$\text{for } 0 < T_1 < 3.0 \text{ s} \quad \sigma^C = b_1 \cdot T_1^3 + b_2 \cdot T_1^2 + b_3 \cdot T_1 + b_4 \tag{4}$$

where the coefficients $a_1, \ldots, a_3$ and $b_{1, \ldots}, b_4$ are regression parameters. The values obtained from regression are reported in tables in Bovo et al. (2022).

2.5 Phase 5: derivation of the fragility curve of the whole building

As discussed before, the perimeter and internal frames of precast RC buildings were analysed separately under the hypothesis of flexible floor diaphragm. Due to the lack of continuity and the insufficiency of the connections, typically the roof slab of the existing precast buildings is very flexible in its own plane and is not able to redistribute the seismic actions between the different structural frames. This is a frequent condition observed in many precast buildings of the Emilia region (Savoia et al. 2012; Bovo and Savoia 2021).

Hence, the following assumptions were introduced: (i) the seismic behavior of the internal frames of a precast building, tagged within the same structural category, is assumed to be identical, i.e., if one frame collapses all the other frames of the same typology collapse as well; (ii) the same hypothesis is considered for the perimeter frames of a building; (iii) the behaviours of the internal frames and the perimeter frames are assumed fully independent.

Therefore, for each precast building, it is sufficient to consider one internal frame typology and one perimeter frame typology and, from the combination of their fragilities, the fragility curve of a building is derived. Structural collapse occurs when at least one of its frames reaches one of the collapse conditions. This simplified hypothesis is acceptable within the purpose of a probabilistic large scale damage evaluation, as discussed in the following sections.

3 The case-study area of San Felice sul Panaro (Modena)

3.1 Main characteristics of the buildings

For the large-scale seismic damage scenario assessment, the productive area of San Felice sul Panaro (province of Modena, Emilia Romagna region, with average coordinates 44.83584°, 11.12508°) has been selected as the case study, with reference to 91 precast RC buildings. They were severely damaged by the 29th May 2012 earthquake, which had an epicenter at 4 km from this area (see Fig. 3). Since the area was significantly far from the epicenter of the 20th May 2012 earthquake, no significant cumulative damage effects occurred. Furthermore, a ground-motion recording station (SAN0) was present nearby. The perimeter of the industrial area is highlighted in red in Fig. 3. It is worth noting that the largest industrial buildings in the area were included in the analysis, whereas the smallest buildings and those not damaged by the event were neglected.

The effects of the earthquake on the buildings are clearly visible in Fig. 4: the first aerial picture was taken one year before the main shock and the second one two years after the earthquake. The aerial view in Fig. 5 highlights the 91 buildings in the case-study area. The red markers indicate the 42 buildings collapsed (in accordance with the criteria indicated in the Sect. 2.3) during the 29th May 2012 main shock.

In the pre-earthquake situation, all the 91 buildings featured one story only and had a rectangular shape in plan, with dimensions ranging from 10.0 to 150.0 m, and areas ranging from 150 to 13,700 m^2.

The building heights varied from 3.0 to 10.0 m, the beam spans between 6.0 and 25.0 m, while the roofing elements length between 5.0 m and 30.0 m. The column cross-section dimensions ranged between 25 and 70 cm.
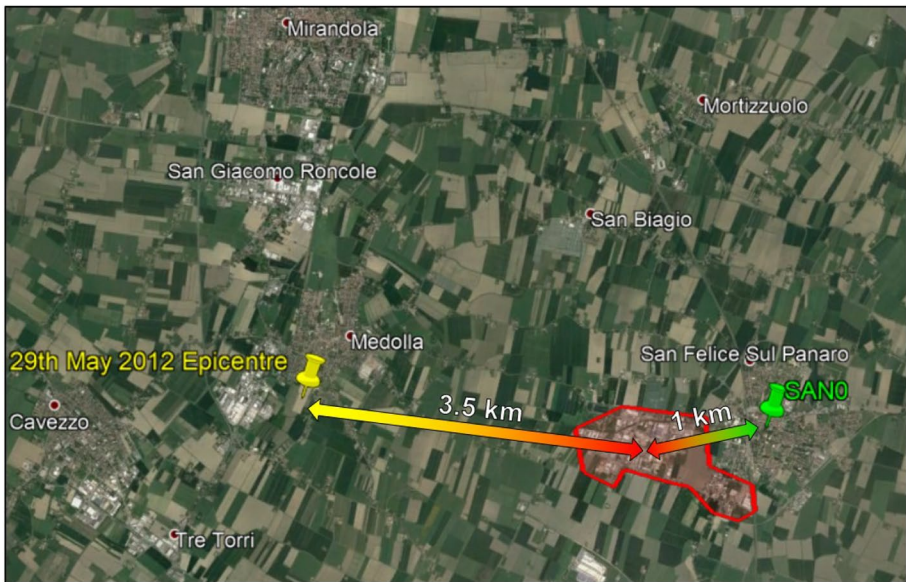

Fig. 3 Google Earth (2021) aerial view: the 29th May 2012 main shock epicenter, the productive area of San Felice sul Panaro (the red polygon), and the ground-motion recording station SAN0

(a) **(b)**

Fig. 4 Google Earth (2021) aerial views of the San Felice sul Panaro main productive area (**a**) before (21 April 2011), and (**b**) after (9 June 2014) the Emilia earthquake of 29th May 2012

Fig. 5 Google Earth (2021) aerial view with the position of the precast buildings. In red the buildings collapsed during the 29th May 2012 main shock

The beam cross-sections were L-shaped, reverse T-shaped, tapered I-shaped, constant I-shaped, H-shaped, Y-shaped, Ω-shaped and shed beams. The floor slab element cross-sections were double tee shape, Y-shaped, rectangular box, hollow cored, channel shaped, wing shaped and shed elements.

3.2 Observed damage

The damage severity for each building was defined based on both accurate building inspections in the aftermath of the earthquake, and on information available form technical documents issued for obtaining public funds for the post-earthquake reconstruction.

In many cases, the main frames of the buildings had significant horizontal relative displacements at the roof level, causing damage to the connections or the loss-of-support

collapse of the beams and roof slab elements (see Fig. 6a–c). In some buildings, the unseating failure of beams and roofing elements did not occur, but large residual displacements were visible (see Fig. 6d). Moreover, damage to the cladding walls was also common, involving cracks or overturning of infill masonry walls (see Fig. 6g, h) or detachment of precast RC cladding panels (see Fig. 6i–l) because of the failure of the connections. Damage mechanisms associated with the formation of plastic hinges at base of columns were observed in a few cases, with concrete cover expulsion, wide cracks and considerable deformations of the longitudinal bars (see Fig. 6e, f), sometimes with bar buckling.

It is worth noting that most of the existing precast RC buildings did not exhibit a ductile behavior under the seismic action but a fragile one (Liberatore et al. 2013; Belleri et al. 2014; Buratti et al. 2017; Savoia et al. 2017). Hence, the damage accumulation due to multiple seismic shocks is not as relevant as it could be for other structural typologies. As a result, the industrial area under analysis was mainly and significantly damaged by the seismic event occurred on the 29th May 2012, and only slightly by the previous shocks.

3.3 Classification of the frames

The first step for the application of the PRESSAFE-disp method is the attribution of a proper category to the frames of each building, based on the taxonomy reported in Fig. 2. A frame class is considered representative of frames which share an equivalent column capacity, the type of structural connections and the type of cladding (if present), but which can have different natural periods of vibration due to the stiffness and mass distributions.

In the case-study, all the necessary structural details (e.g. geometry, dimensions, beam and roof element typology, column cross-section, material properties, connections, cladding etc.) were deduced from the documents available, or detected during the visual inspections. The frame categories selected for each of the 91 precast buildings are reported in Table 1. Three buildings did not have internal frames (due to their small dimensions) and three did not have perimeter frames since they were used as open storage areas. The symbols used for the classification are explained in Sect. 2.1. In few cases, the documentation was incomplete, and the missing parameters were assumed by engineering judgements based on similarities with other buildings. Moreover, in some cases it was not possible to establish if the collapse occurred in the internal, perimeter or in both the frame types. This aspect is taken into account in the development of the large-scale probabilistic calculation which considers a distinct seismic behaviour of the frames of the building, as further explained in the following section.

The internal and perimeter frame categories, adopted for the 91 buildings in the case-study area, are illustrated in Fig. 7a–d. The disaggregation of the classification criteria of the frame categories is plotted in Fig. 7e and f. The internal frames were classified into 13 categories, reported in the pie plot in Fig. 7a, whose values represent the number of frames belonging to each category. Among the internal frames, 46 of them were associated to the lowest flexural capacity of columns (A), while 21, 20 and 1 were classified as (B), (C) and (D), respectively (see Fig. 7e). On the other hand, 23 categories were used to classify the perimeter frames, which are represented in separated pie graphs based on the cladding typology (see Fig. 7b–d). Most of the perimeter frames, i.e., 42, had infill masonry walls (m), 29 frames had RC horizontal cladding panels (h2), and 17 frames had RC vertical cladding panels (v) (see Fig. 7f). Most of the frames had friction-based supports (code (L), meaning low strength). In particular, 67 frames featured this type of support in the beam-column connections and 79 frames in the roof-beam connections.

Fig. 6 Collapse and damage mechanisms observed in the buildings of the case-study area of San Felice

Regarding the beam-column connections, 14 frames were classified as medium-strength connection type (M), whereas 7 frames as high strength connection type (H). Finally, only 9 frames had roof-beam connections classified as (H), i.e., high strength. It is important to

Table 1 Main parameters of the 91 precast RC buildings considered in the study

#	Surface (m^2)	Column height (m)	Beam length (m)	T_1 (s) perimeter frame	T_1 (s) internal frame	Internal frame class	Perimeter frame class	Building collapsed
1	1276	7.2	21.1	1.07	0.76	C-L-L-I	C-L-L-P (m)	Y
2	389	5.0	19.7	0.92	0.65	A-M-L-I	A-M-L-P (v)	N
3	182	5.3	15.0	/	0.58	/	A-M-L-P (v)	N
4	387	5.3	15.0	0.70	0.50	A-M-L-I	A-M-L-P (v)	N
5	336	6.4	14.0	1.11	0.78	B-L-L-I	B-L-L-P (m)	Y
6	392	6.2	14.6	0.45	0.32	C-L-L-I	C-L-L-P (h2)	Y
7	140	4.5	9.4	0.45	0.32	B-M-L-I	B-M-L-P (h2)	Y
8	834	6.5	8.9	0.81	0.58	B-M-H-I	B-M-H-P (h2)	N
9	1617	6.0	16.4	1.04	0.73	B-M-H-I	B-M-H-P (m)	N
10	4958	8.6	19.5	1.88	1.83	B-M-L-I	B-M-L-P (h2)	N
11	1068	6.9	12.6	1.48	1.05	A-L-L-I	A-L-L-P (m)	Y
12	1280	7.0	16.0	1.56	1.10	A-L-L-I	A-L-L-P (m)	N
13	561	7.0	18.3	1.60	1.13	A-L-L-I	A-L-L-P (m)	Y
14	254	5.3	10.1	0.79	0.56	A-L-L-I	A-L-L-P (m)	N
15	714	5.0	17.0	0.60	0.43	A-M-L-I	A-M-L-P (m)	N
16	714	5.0	17.0	0.82	0.58	A-M-L-I	A-M-L-P (m)	N
17	3647	6.5	6.0	0.66	0.47	A-H-L-I	A-H-L-P (m)	N
18	1404	5.5	13.0	0.52	0.37	A-L-L-I	A-L-L-P (m)	Y
19	1855	5.9	20.3	0.85	0.60	A-L-L-I	A-L-L-P (m)	N
20	1115	3.8	20.4	0.44	0.31	A-L-L-I	A-L-L-P (v)	Y
21	896	4.5	10.5	0.46	0.33	A-M-H-I	A-M-H-P (v)	N
22	307	6.9	16.8	1.63	1.15	A-M-L-I	A-M-L-P (m)	N
23	1230	8.5	20.5	1.03	0.73	C-L-L-I	C-L-L-P (h2)	Y
24	820	8.5	20.5	1.03	0.73	C-L-L-I	C-L-L-P (h2)	Y
25	236	10.0	20.5	–	0.93	–	C-L-L-P (m)	N
26	2460	8.5	20.5	1.78	1.26	C-L-L-I	C-L-L-P (h2)	N
27	684	4.7	19.0	0.59	0.42	C-L-L-I	C-L-L-P (v)	Y
28	570	6.1	19.0	1.29	0.92	A-L-L-I	A-L-L-P (h2)	N
29	4104	7.1	18.0	1.61	1.14	A-L-L-I	A-L-L-P (m)	N
30	2687	8.0	11.0	1.47	1.04	B-L-L-I	B-L-L-P (h2)	Y
31	3514	8.0	17.5	1.25	0.88	B-L-L-I	B-L-L-P (h2)	Y
32	1464	6.0	15.0	1.08	0.76	A-L-L-I	A-L-L-P (h2)	Y
33	251	4.6	10.6	1.19	0.84	A-L-L-I	A-L-L-P (m)	N
34	627	5.0	14.0	0.54	0.38	B-L-L-I	B-L-L-P (m)	N
35	161	7.6	12.8	1.15	0.81	A-L-L-I	A-L-L-P (m)	N
36	384	6.7	12.8	1.17	0.82	A-L-L-I	A-L-L-P (m)	N
37	161	7.6	12.8	1.15	0.81	A-L-L-I	A-L-L-P (m)	N
38	384	6.7	12.8	1.17	0.82	A-L-L-I	A-L-L-P (m)	N
39	7378	8.9	13.0	1.07	0.75	C-L-L-I	C-L-L-P (v)	N
40	13,750	4.5	15.7	0.50	0.35	A-L-L-I	A-L-L-P (m)	Y
41	2379	9.3	20.0	1.19	–	C-L-L-I	–	Y
42	7752	6.0	8.5	0.73	0.51	B-L-L-I	B-L-L-P (h2)	Y
43	1380	7.6	15.0	1.36	–	C-M-H-I	–	N

Table 1 (continued)

#	Surface (m²)	Column height (m)	Beam length (m)	T_1 (s) perimeter frame	T_1 (s) internal frame	Internal frame class	Perimeter frame class	Building collapsed
44	4484	8.0	5.9	0.83	0.59	B-L-L-I	B-L-L-P (h2)	Y
45	5400	7.6	8.5	1.76	1.24	C-M-H-I	C-M-H-P (v)	N
46	1596	8.0	8.0	0.89	0.63	B-L-L-I	B-L-L-P (v)	Y
47	2542	7.7	10.0	–	1.21	–	C-M-H-P (h2)	N
48	902	4.3	18.5	1.18	0.83	A-L-L-I	A-L-L-P (m)	Y
49	434	5.9	14.2	1.09	0.77	A-L-L-I	A-L-L-P (m)	N
50	337	5.9	14.1	1.07	0.76	A-L-L-I	A-L-L-P (m)	N
51	551	7.9	18.1	1.89	1.34	A-L-L-I	A-L-L-P (m)	Y
52	954	7.1	22.5	1.11	0.79	A-L-L-I	A-L-L-P (m)	N
53	827	3.6	18.6	0.63	0.44	A-L-L-I	A-L-L-P (h2)	N
54	2373	6.6	12.0	1.34	0.95	A-L-L-I	A-L-L-P (m)	Y
55	506	6.5	21.0	0.84	0.68	B-L-L-I	B-L-L-P (h2)	N
56	566	6.0	18.7	0.55	0.39	C-L-L-I	C-L-L-P (h2)	Y
57	756	6.5	14.0	0.92	0.65	A-L-L-I	A-L-L-P (h2)	N
58	675	7.0	22.2	1.22	0.86	A-H–L-I	A-H–L-P (m)	N
59	3986	8.1	10.0	1.48	1.04	C-H–H-I	C-H–H-P (v)	N
60	1952	5.8	16.0	0.66	0.47	B-L-L-I	B-L-L-P (m)	Y
61	1080	5.0	15.0	0.82	0.60	A-L-L-I	A-L-L-P (m)	Y
62	405	4.0	7.5	0.22	0.16	B-L-L-I	B-L-L-P (v)	Y
63	1088	5.3	20.0	0.57	0.40	B-L-L-I	B-L-L-P (v)	Y
64	935	5.8	8.7	0.58	0.41	B-L-L-I	B-L-L-P (h2)	Y
65	300	6.2	10.0	0.52	0.37	B-L-L-I	B-L-L-P (m)	Y
66	300	6.2	15.0	0.82	0.58	C-L-L-I	C-L-L-P (m)	N
67	880	4.5	11.0	0.65	0.46	C-L-L-I	C-L-L-P (h2)	Y
68	2442	5.9	9.3	0.86	0.61	A-L-L-I	A-L-L-P (h2)	Y
69	656	4.5	15.5	1.44	1.02	A-L-L-I	A-L-L-P (m)	N
70	419	6.5	17.2	1.03	0.73	A-L-L-I	A-L-L-P (h2)	Y
71	410	6.5	16.8	1.03	0.72	A-L-L-I	A-L-L-P (m)	Y
72	2604	6.7	10.0	1.04	0.74	C-H-H-I	C-H-H-P (h2)	N
73	750	6.0	15.0	1.09	0.77	B-H-H-I	B-H-H-P (m)	N
74	581	7.0	18.5	1.06	0.75	A-L-L-I	A-L-L-P (v)	N
75	1810	7.0	18.1	0.95	0.84	A-L-L-I	A-L-L-P (v)	N
76	1806	5.2	12.5	0.80	0.57	C-H-H-I	C-H-H-P (v)	Y
77	2020	7.0	19.0	1.38	0.96	B-M-L-I	B-M-L-P (h2)	N
78	1791	7.0	20.0	1.29	0.91	B-L-L-I	B-L-L-P (h2)	Y
79	1000	6.0	19.7	1.38	0.98	A-L-L-I	A-L-L-P (m)	Y
80	678	6.8	16.0	0.93	0.66	B-L-L-I	B-L-L-P (m)	Y
81	5971	10.0	23.0	1.52	1.08	D-L-L-I	D-L-L-P (h2)	Y
82	1909	9.1	16.5	1.32	0.93	A-L-L-I	A-L-L-P (m)	Y
83	3070	7.1	20.2	1.67	1.18	A-L-L-I	A-L-L-P (m)	N
84	263	4.2	6.2	0.42	–	A-L-L-I	–	Y
85	495	4.6	10.0	0.49	0.35	A-L-L-I	A-L-L-P (m)	N
86	2358	9.5	20.5	1.07	0.76	A-L-L-I	A-L-L-P (m)	Y

Table 1 (continued)

#	Surface (m²)	Column height (m)	Beam length (m)	T_1 (s) perimeter frame	T_1 (s) internal frame	Internal frame class	Perimeter frame class	Building collapsed
87	581	6.3	16.4	0.72	0.51	A-L-L-I	A-L-L-P (h2)	N
88	320	6.8	16.4	0.67	0.47	C-L-L-I	C-L-L-P (h2)	N
89	389	6.3	11.8	0.47	0.33	C-L-L-I	C-L-L-P (h2)	N
90	900	4.0	6.5	0.26	0.18	C-L-L-I	C-L-L-P (v)	Y
91	1350	4.0	6.5	0.26	0.18	C-H-L-I	C-H-L-P (v)	N

notice that the widespread adoption of friction-connections and the low moment-capacity of columns are mainly due to the lack of seismic design criteria for the buildings in the area under consideration, classified as non-seismic until 2003.

3.4 Fragility curves

The PRESSAFE-disp method defines the seismic fragility of each frame class as a function of the natural period of vibration, as discussed in Sect. 2.4. This parameter is calculated for each frame considering the columns as cantilevers. This simple structural scheme is acceptable in one-storey precast buildings, in which usually the roof does not constitute a rigid diaphragm, as reported for example in Minghini et al. (2016). Therefore, the lateral stiffness K_f of each frame was computed as:

$$K_f = \sum_i K_{c,i} = \sum_i 3E_c J_i / l_i^3 \tag{5}$$

where $K_{c,i}$, J_i, and l_i are the lateral stiffness, the second moment of the cross-section and the length of the i-th column, respectively, and E_c is the Young modulus of concrete.

The mass adopted to calculate the natural period was estimated from load analysis. The natural periods of the internal and the perimeter frames of all the buildings in the case-study area are reported in Table 1. Coherently with the method described in Bovo and Savoia (2021), the periods of vibration are determined considering the bare frames, i.e., not considering the presence of the cladding elements.

After the classification of the frames of the buildings and the calculation of their natural period of vibration, the parameters of the collapse fragility curve for each frame (see Tables 6 and 7 in Appendix) were computed using Eqs. (2)–(4) and the values reported in Bovo et al. (2022).

The fragility curves obtained by means of the PRESSAFE-disp method are plotted in Fig. 8a, b for the internal and perimeter frames, respectively. The average curves, estimated with the method of Shinozuka et al. (2000), are represented with a red line. The figures show that the fragility curves of the internal frames are less scattered than those of the perimeter frames. This is, in part, due to the fact that the perimeter frames have a strong variability due to the different type of cladding, i.e., infill masonry walls, horizontal RC cladding panels and vertical RC cladding panels. Moreover, in general, the fragility curves for the internal frames are characterized by lower median values (i.e., the values corresponding to PoE equal to 0.5) than those for perimeter frames (e.g., ranging from 0.1 to 0.5 g for the internal frames and from 0.25 to 1.25 g for perimeter frames). The higher value of capacity (considering the median value) of the perimeter frames is due to the presence of cladding elements.
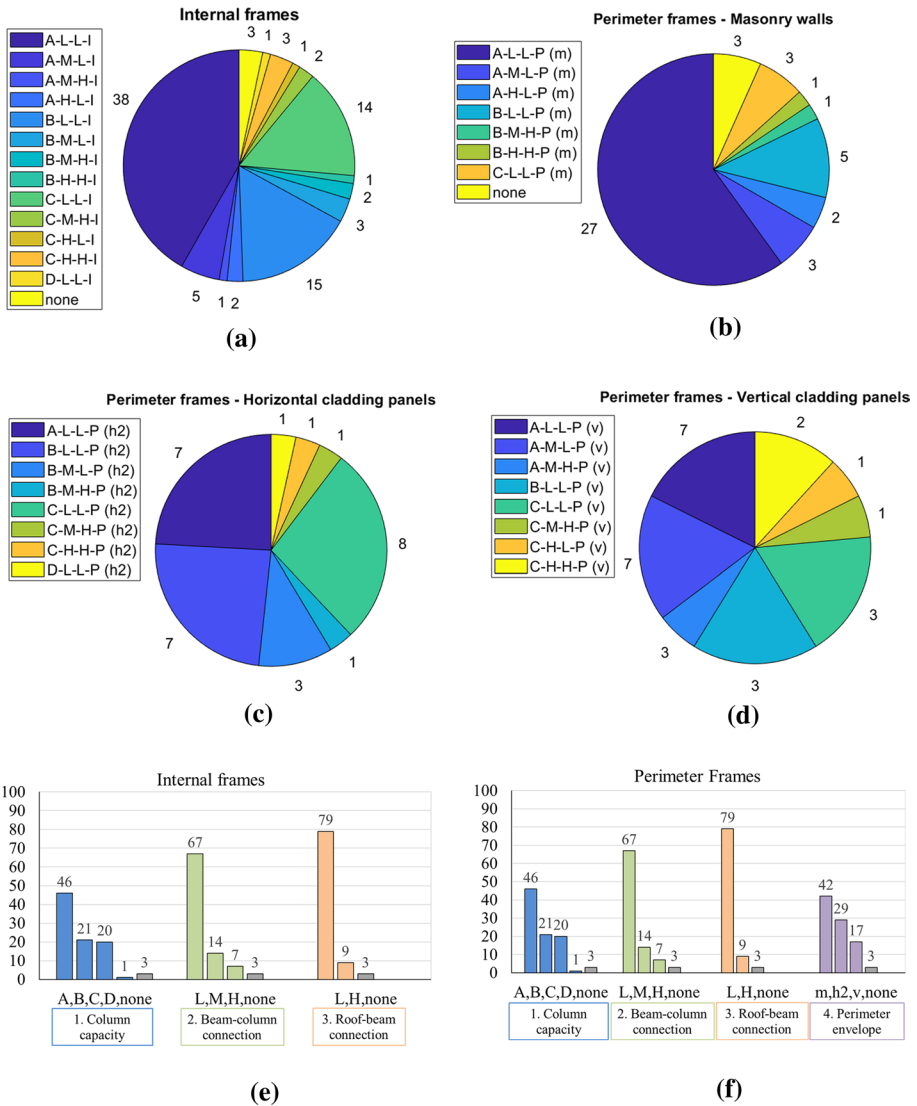
Fig. 7 Classification of the 91 buildings in San Felice industrial area: **a** internal frames; **b** perimeter frames with masonry infills; **c** perimeter frames with precast RC horizontal cladding panels; **d** perimeter frames with precast RC vertical cladding panels. Disaggregation of the **e** internal frames and **f** perimeter frames, following the four criteria of PRESSAFE-disp

4 Assessment of the damage scenario

Starting from the outcomes discussed in the previous section, a large-scale seismic damage scenario assessment was performed. In particular, the parameter considered for the evaluation of the soundness of the PRESSAFE-disp method was the number of collapsed buildings resulting from the application of the method, in comparison with the actual number of collapsed buildings in the area, i.e., 42.

For the definition of the seismic risk of a building, two input models must be established: (i) the fragility model and (ii) the seismic input model. The former has been already discussed and derived from the application of the PRESSAFE-disp method, whereas the latter is described in detail in the following.

The seismic input model depends on the type of analysis to perform. A scenario analysis to forecast the consequences of a possible future event may require the definition of a probabilistic seismic input model (e.g. shake map, Worden et al. 2018), given for instance the source-to-site distance and the earthquake magnitude (FEMA 2018). In the present study, in order to compare the output with the actual post-event data (the number of collapsed buildings), the seismic input was assumed deterministic, due to the availability of the ground-motion recordings of May 29th 2012 earthquake by the SAN0 station, located very close to the industrial area (about 1 km, see Fig. 3). Hence, three different deterministic seismic input models were defined from the ground-motion recordings, see Sect. 4.1. Subsequently, two procedures have been adopted to combine statistically the fragility model and the seismic input model. The first procedure adopted was based on Monte Carlo simulation (MC) (Sect. 4.2), while the second approach is a Direct Simplified (DS) calculation (Sect. 4.3), aimed at the fast evaluation of the number of collapsed buildings.

4.1 Ground-motion intensity

The industrial area under consideration was selected not only because of the availability of data on the precast buildings, but also because there was a ground-motion recording station (SAN0) at a distance shorter than 1 km, allowing to strongly reduce the uncertainty on the ground-motion intensity of the 29th May 2012 earthquake. Nevertheless, some uncertainties remain because of:

1.   the attenuation of the ground-motion which can be fast in the near-field region;
2.   the directionality of the ground-motion which was significant for the earthquake under consideration and for the planar precast RC buildings considered (Savoia et al. 2017).

The first uncertainty source was neglected in the present study, thus assuming that the ground-motion recorded by the SAN0 station corresponds to that in the industrial area, because both the sites are on the surface projection of the fault (same Joyner-Boore source-to-site distance) and the geological conditions of the area are uniform (Dolce et al. 2012).

The second uncertainty source was considered, with different levels of approximation. In particular, starting from the North–South and East–West acceleration records registered during the 29th May 2012 main shock at the recording station SAN0 (Itaca database), three seismic inputs (SIN) models were considered:

•   SIN1: pseudo-acceleration response spectrum S_a with 5% damping, calculated as the maximum value between the two SAN0 spectra in the North–South and East–West directions;
•   SIN2: pseudo-acceleration response spectrum S_a with 5% damping, calculated as the geometric mean of the two SAN0 spectra in the North–South and East–West directions;

- SIN3: pseudo-acceleration response spectrum S_a with 5% damping, calculated according to the orientation of the main frames for each building; in this case, the response spectrum can be different for each building.

The three different seismic input, from SIN1 to SIN3, would represent a series of progressive refinements and improvements of the seismic input model. Theoretically, the SIN3 should provide the best assessment among the three approaches considered, because the behavior of the precast RC buildings tends to be very different in the directions of main frames and orthogonally to them. To this regard, it is worth noting that the PRESSAFE-disp method is a simplified method which considers only the behavior in the plane of the main frames. Therefore, theoretically, the ground accelerations in the direction of the main frames should be considered as in SIN3. However, the directionality of the ground-motion is normally not available in forecast damage scenarios since reliable predictive models have not yet been developed. Indeed, in those cases, the seismic inputs are usually in the form of SIN1 or SIN2, and not SIN3. Hence, even if the adoption of SIN3 is expected to give the most reliable output in the simulation of the past event of the 29th of May 2012, SIN1 and SIN2 were also tested to explore the sensitivity of the results to the ground-motion directionality.

The pseudo-acceleration response spectra adopted in models SIN1 and SIN2 are plotted in Fig. 9. To show the directionality of the ground-motion, considered in the model SIN3, Fig. 10a reports the pseudo-accelerations for $T=0$ s, $T=0.5$ s, $T=1.0$ s, $T=1.5$ s and $T=2.0$ s, along different orientations. Angles are measured with respect to the East direction and increase towards North. In Fig. 10a, the values at $T=0$ s correspond to the Peak Ground Acceleration (PGA), with maximum equal to 0.226 g and minimum equal to 0.170 g. For $T=0.5$ s, the maximum pseudo-spectral acceleration among all the horizontal directions is 0.750 g, while the minimum is 0.317 g; for $T=2.0$ s the maximum and minimum spectral accelerations are 0.236 g and 0.073 g, respectively.

The orientation of the main frames of the 91 buildings under consideration is reported in Fig. 10b. Clearly, there are two clusters of buildings, one with main frames with orientation of about 70° from East and one of 160° from East.

4.2 Monte Carlo (MC) simulation

The Monte Carlo simulation is a highly repetitive process in which the result, in this case the number of collapsed buildings, is calculated performing a large number of numerical simulations (Grigoriu 2002). This method is used to estimate a distribution of possible outcomes starting from a set of random input data; it results in a rather complex procedure which is computationally expensive because of the need of many simulations. On the other hand, the Monte Carlo simulation is very powerful because it can be applied to different types of uncertainty models (e.g. parametric, non-parametric, continuous variables, discrete variables, etc.) and to non-linear models. Moreover, the final result is a statistical distribution of outcomes, which can be used to calculate not only the most likely event, but also the uncertainty in the event of interest.

4.2.1 Simulation of damage scenarios

In the present case, in order to consider the epistemic uncertainty on the behavior of buildings (e.g., uncertainties in selecting an appropriate structural model, as well as uncertainties

in the measurement of physical quantities or lack of sufficient data, see Sects. 2 and 3), the natural period of the perimeter and the internal frames was considered uncertain. A uniform probability distribution in the interval $[(1-\alpha)T_1, (1+\alpha T_1]$ was used to this aim, where T_1 indicates the estimate of the period reported in Table 1 and α is a building-dependent parameter, set to either 0.1, 0.2 or 0.3, based on the quality and amount of data available. In the simulations, the periods of the internal and perimeter frame of the same building were considered uncorrelated. As already mentioned in Sect. 2.5, since precast buildings are conceived as systems of independent frames when designed without seismic provisions, the seismic behavior of the two frame typologies was analysed separately, and then the results were combined in a subsequent stage. When a frame typology (either internal or perimeter) was not present in a building, its fragility was based on the characteristics of the only frame type in the structure.

The following steps summarize the calculations performed in each of the MC simulations. The procedure was implemented in a Matlab (MathWorks 2020) script:

For each frame of each building, a value of the natural period is randomly sampled from a uniform distribution in the interval $[(1-\alpha)T_1, (1+\alpha T_1]$, where T_1 is the estimate of the natural period reported in Table 1, and α is a building-dependent parameter, set to either 0.1, 0.2 or 0.3, based on the quality and amount of data available;

Given the period of each frame, the corresponding fragility curve is determined using the parametric fragility surfaces of the PRESSAFE-disp method (see Sect. 2.4);

Given the period of each frame, the corresponding S_a value is determined from the selected seismic input model (i.e., either SIN1, SIN2 or SIN3);

For each frame, the probability of collapse is calculated through the fragility curves (defined in step 2) with the spectral acceleration computed at step 3;

To determine if a frame collapses, a random value is sampled from a continuous uniform distribution in the interval [0;1] and compared with the probability of collapse computed at step 4. If the sampled random number is smaller than the probability of collapse (step 4), the frame is considered collapsed, and a value equal to 1 is assigned. Otherwise, if the sampled random number is higher than the probability of collapse, the frame is considered not collapsed and a 0 is assigned. This approach follows the recommendations given in FEMA (2018), considering the event "frame collapse" as a discrete Bernoulli random variable;

A building collapses if either the internal frame or the perimeter frame collapses (if one of the frames, or both, is assigned a 1);

The procedure 1–6 is repeated for all the 91 buildings, and the total number of collapsed buildings is computed.

In the present work, a total of 100,000 simulations were performed. Figure 11 shows the results obtained, in terms of number of collapsed buildings, adopting the previously described seismic input models in step 3, i.e. SIN1, SIN2 and SIN3. The vertical axis of the plot indicates the relative frequency of the number of collapsed buildings in the simulations, normalized in order to have a unitary total area of the histogram. From the literature (Benjamin and Cornell 1970), the central limit theorem indicates that the distribution of the sum of a large number of uniformly distributed independent random variables approaches the normal distribution. Thus, the fitting functions adopted in Fig. 11 are normal distributions, represented with a continuous black line. Figure 11 shows that the dispersions (σ) of the three distributions are essentially equivalent, whereas the expected (i.e. mean) value (μ) of collapsed building changes, from about 57 for SIN1, to 47 for SIN2 and for SIN3.

The parameters of the best fitting normal distributions are given in Table 2 for the three seismic input models considered, together with the relative prediction error (E_R), in percentage, calculated with reference to the actual number of collapsed buildings occurred during the seismic event ($N_{c,act}=42$, indicated with a red line in Fig. 11).

The different intervals marked with dashed lines in the Figure represent the "three-sigma" rule of the normal distribution (Fisz 1963). The three intervals, reported in Table 2, contain the 68.3%, the 95.5% and the 99.7% of the samples around the mean value. Since the distributions of the predicted data approach the normal one, which is highly concentrated around the expected value, the probability that the data differs from the mean value by more than 2σ is less than 5%, for each distribution. Since the mean value is the reference result of the large-scale MC analysis, the intervals provide an indication of the dispersion of the values from the mean one, which is a measure of the uncertainty in the prediction.

The MC simulations with the three different seismic input models resulted in a slightly higher number of collapses if compared with the actual effect of the earthquake. This result could be somehow expected, due to the simplifying conservative assumptions introduced in the numerical simulations of the PRESSAFE-disp method (for instance the strength of some non-structural elements was neglected). Nevertheless, the rather small errors indicate that the fragility surfaces proposed may provide a quite reliable representation of the seismic behavior of precast RC buildings, when the goal is the evaluation of damage scenarios at the territorial scale.

The most accurate outcomes were obtained by adopting the seismic inputs SIN2 and SIN3, i.e., considering the geometric mean of the two N-S and W-E spectra of the recorded accelerations (SIN2) and the spectra in the direction of the main frame of each building (SIN3), respectively. Indeed, from Fig. 11 it is evident that the line marking the actual number of collapses is within the 2σ interval around the mean value for SIN2 and SIN3, while it lays outside the 3σ interval for SIN1.

Other interesting remarks can be drawn considering the geographical orientation of the buildings. Indeed, as mentioned before, the buildings of the case-study area can be sorted in two groups according to their main frame orientations, with average values of about 70° and 160° respectively, measured from East (see Fig. 10b). The mean values of the spectral accelerations for the two groups of buildings, for each seismic input, are represented in Table 3, for both internal and perimeter frames. The S_a values are strongly dependent on the frame orientations, and the SIN2 and SIN3 models are on average in good agreement for both type of frames, featuring lower values compared to SIN1, as expected. Moreover, the average spectral accelerations of the perimeter frames are higher compared to the ones of the internal frames for all seismic inputs, due to the different values of natural periods (see Table 1).

Table 4 reports the average number of collapses in the 100,000 Monte Carlo simulations, for the two groups of buildings with different orientation. The sum of the number of collapses provided in Table 4 corresponds to the mean values reported in Table 2, for each seismic input considered. As mentioned before, the adoption of SIN1 leads to a higher number of collapses with respect to the other two seismic inputs. It is worth noticing that there is not a remarkable difference between the outcomes of the two groups of buildings in terms of number of collapses, since a mixed population of frame categories, with a significantly different seismic behavior, is included in both groups.

All these results, on one hand, suggests that the seismic input SIN1, calculated as the maximum between the two spectra recorded in the SAN0 station, is too conservative, on the other

	μ (–)	σ (–)	E_R (%)	$\mu \pm \sigma$ (–)	$\mu \pm 2\sigma$ (–)	$\mu \pm 3\sigma$ (–)
SIN1	57.3	3.9	+36.5	53.4÷61.2	49.6÷65.1	45.7÷69.0
SIN2	46.7	4.2	+11.2	42.5÷50.9	38.3÷55.1	34.1÷59.2
SIN3	46.9	4.1	+11.7	42.9÷51.0	38.8÷55.1	34.7÷59.1

Table 2 Main descriptors of best fitting normal distribution illustrated in Fig. 11, and relative prediction error, for three different seismic inputs

hand, they prove that the adoption of the PRESSAFE-disp fragilities, together with an appropriate seismic input, could represent a reliable tool for the damage scenario assessment of precast RC buildings. Even though the seismic input SIN2 is obtained through a rather simple calculation, its application is much simpler with respect to SIN3 because it does not require to consider the directionality of the ground-motion, which can be very complex, in general, due to the lack of reliable models in the literature. Nevertheless, the MC outcomes show that SIN2 could be effectively adopted to obtain a realistic assessment of the number of collapsed buildings.

4.2.2 Disaggregation of the results

Figure 12 shows the disaggregation of the outcomes of the MC simulations considering the seismic input model SIN3. In particular, the histograms represent the frequency of occurrence of the collapse condition, of internal and perimeter frames, and of the whole buildings in the 100,000 simulations. With reference to the steps of analysis described before, Fig. 12a illustrates the disaggregation of the outcomes obtained at step 5, whereas Fig. 12b shows the results obtained at step 6. On average, the perimeter frames showed a lower collapse attitude than internal frames, because they can benefit from the presence of non-structural walls/panels. It is worth noticing that each histogram in Fig. 12b, representing the frequency of occurrence of collapse for the 91 precast buildings, is at least as high as the highest histogram representing the collapse of the corresponding frames (see Fig. 12a), in accordance with the hypothesis of the calculation defined at step 6.

In Fig. 13 the outcomes of the MC simulation (for the seismic input SIN3) are disaggregated for each building. The coloured cylinder, located in correspondence of each building position in the map, represents the predicted collapse attitude of the precast structure out of the whole set of simulations. The collapse occurrence is graphically represented by means of the height and the colour of the cylinder: the red cylinders represent the buildings with a frequency of occurrence of collapse higher than 75%; the green cylinders a frequency lower than 25%; yellow cylinders a frequency from 25 to 50% and orange cylinders in the range 50% to 75%.

The results of Fig. 13 can be qualitatively compared with the map in Fig. 5, in which the red marks indicate the exact positions of the collapsed buildings in the seismic event considered, with the aim of verifying the accuracy of the results not only at the "large-scale" point of view (total number of buildings collapsed in the area) but also at the point of view of the specific building (single precast building). This comparison shows that the outcomes of the MC simulation are, on average, in good agreement with the in-field data of real collapses for most of the buildings investigated. However, in some cases the simulation was not able to identify correctly the collapse occurred, in particular for buildings having a seismic capacity very close to the seismic demand. Moreover, for buildings with irregularities highly affecting the seismic behavior, the method proposed could lead to a wrong estimation of the seismic capacity. Of course, a more refined and time-consuming modelling strategy of each individual building could improve the final result, however, it would require the deep knowledge of the geometrical and material characteristics of them (Belleri et al. 2015; Nastri et al. 2017; Dal Lago and Ferrara 2018; Magliulo et al. 2018; Bovo and Savoia 2018; Bovo and Savoia 2019; Dal Lago et al. 2019; Brunesi et al. 2020; Soydan et al. 2020), and it could be not appropriate for a large-scale seismic damage assessment.

4.3 Direct simplified (DS) calculation

A Direct Simplified (DS) and fast calculation is also proposed here with the aim of conducting a preliminary estimation of the number of collapses at the territorial scale. The method is deemed to be alternative and simpler with respect to that based on the Monte Carlo (MC) simulation. Moreover, the epistemic uncertainties on the natural period of buildings are not included in this process.

The DS calculation has been performed considering the same three seismic input models, i.e. SIN1, SIN2 and SIN3, adopted for the MC simulation. The mathematical procedure is based on the fundamental axioms of the probability theory and the algebra of datasets (Benjamin and Cornell 1970).

Considering the case-study building stock, the input data of the problem were the categories selected for the internal and the perimeter frames of each precast RC building, and the corresponding natural periods reported in Table 1. The parameters (i.e. median and standard deviation) of the lognormal fragility curves were calculated by means of the PRESSAFE-disp fragility surfaces (see Sect. 2.4), for the perimeter and internal frames of the 91 buildings in the stock. The collapse fragility curves are those shown in Fig. 8, obtained considering that the periods of vibration were deterministic.

With reference to a specific precast RC building, the failures of the various frames of the same type are assumed to occur at the same time. Hence, only one internal frame and one perimeter frame were considered. Given the natural period of each frame, the corresponding pseudo-spectral acceleration S_a was obtained from the seismic input model and then, through the fragility curves, the probability of collapse was computed for each frame. In the following, the collapse probability of the internal frame and of the perimeter frame of the i-th building are indicated as $P_i(E_I)$ and $P_i(E_P)$, respectively. With reference to a general building, these two probability values are considered associated with two random events, i.e., the collapse of the internal frames and the collapse of the perimeter frames, assumed statistically compatible (i.e. non-mutually exclusive) and statistically independent, following the hypothesis of flexible roof. Therefore, the collapse of a building occurs if one of the internal or perimeter frames collapses, or both; and the collapse of the two frame types (internal and perimeter) can occur at the same time, meaning that the probability of the intersection of the events is not zero. As a result of these hypotheses, the probability of the union of the two events, representing the collapse probability of the i-th building, can be calculated with the generalized additivity axiom:

$$P_{B,i} = P_i(E_I \cup E_P) = P_i(E_I) + P_i(E_P) - P_i(E_I \cap E_P) \tag{6}$$

being E_I and E_P the internal and perimeter frame collapse events, respectively. The two events are considered independent and the following expression can be derived:

$$P_{B,i} = P_i(E_I \cup E_P) = P_i(E_I) + P_i(E_P) - P_i(E_I) \cdot P(E_P) \tag{7}$$

Since the lognormal functions do not have the additive regenerative property, but they are characterized by a multiplicative regeneration ability (Benjamin and Cornell 1970), it is not possible to obtain an analytical expression for the fragility of the building as a function of the fragilities of the frames because the result would not be a lognormal function. Thus, the fragility curve of the entire i-th building can be obtained in a discrete form, by calculating the collapse probability $P_{B,i}$ for a set of values of S_a.
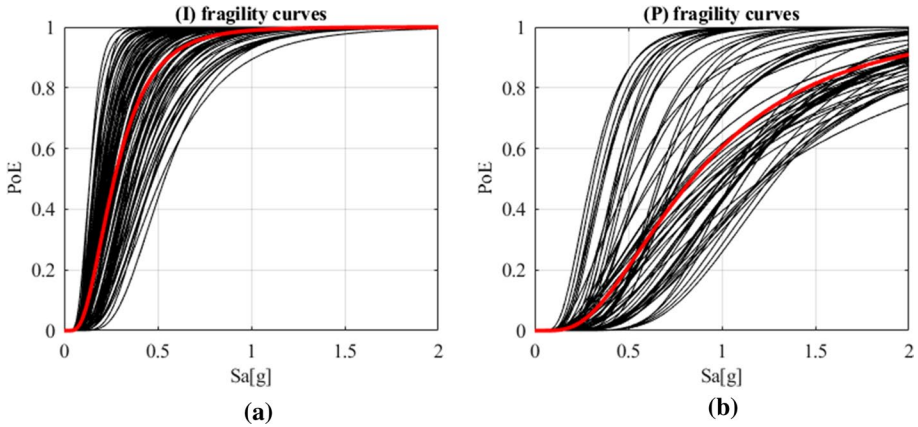
Fig. 8 Fragility curves obtained with the PRESSAFE-disp method for (**a**) internal frames and (**b**) perimeter frames, for the 91 buildings of the case-study area
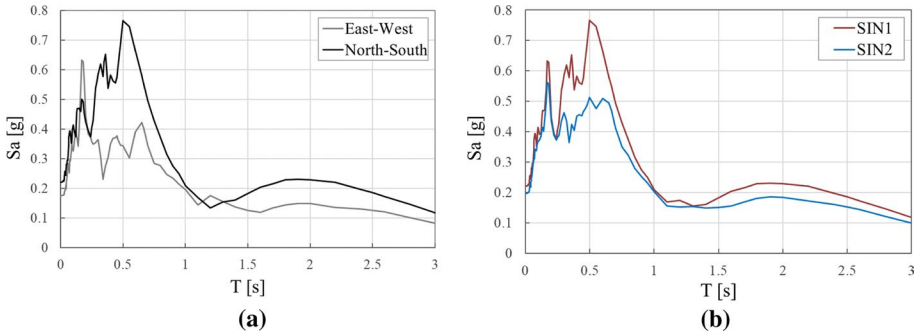

Fig. 9 Acceleration response spectra: **a** East–West and North–South spectra obtained from the recording station SAN0 during the 29th May 2012 main shock; **b** SIN1 and SIN2 response spectra calculated as the maximum and the geometric mean of the two recorded spectra, respectively
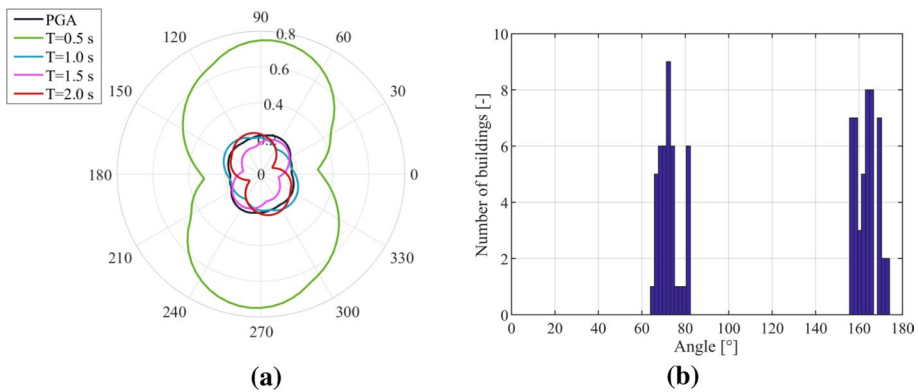

Fig. 10 **a** Pseudo-spectral accelerations in units of g for T=0 s, T=0.5 s, T=1.0 s, T=1.5 s, T=2.0 s, in different directions, and **b** orientation of the main frames for the 91 buildings considered. Angles are measured from East and 90° correspond to North.
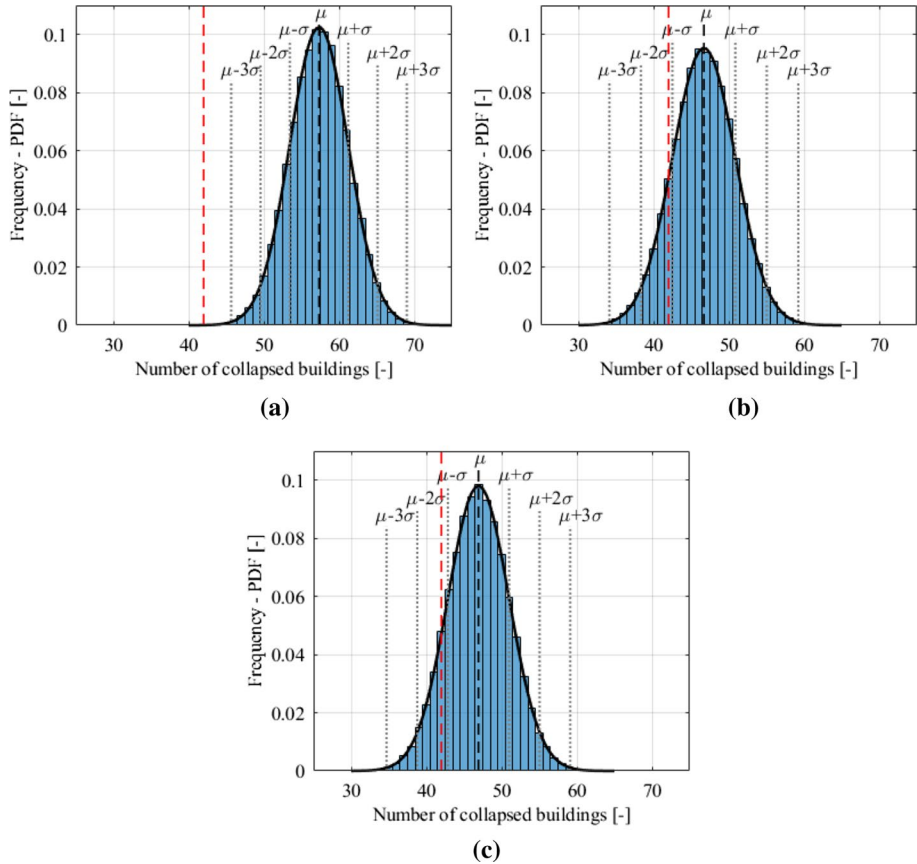
Fig. 11 Prediction of the number of collapsed buildings and best fitting normal distributions for 100,000 Monte Carlo simulations, for three different seismic inputs: **a** SIN1, **b** SIN2 and **c** SIN3. The red line marks the actual number of collapses

Table 3 Mean values of the spectral accelerations of internal (I) and perimeter (P) frames, for the two groups of frames with different average orientations, for the three seismic inputs

	Average orientation 70°		Average orientation 160°	
	S_a (I) (g)	S_a (P) (g)	S_a (I) (g)	S_a (P) (g)
SIN1	0.287	0.440	0.354	0.438
SIN2	0.241	0.356	0.288	0.340
SIN3	0.262	0.402	0.264	0.300

Table 4 Number of collapses of the precast buildings estimated in the Monte Carlo simulation, for the two groups of frames with different average orientations, for the three seismic inputs

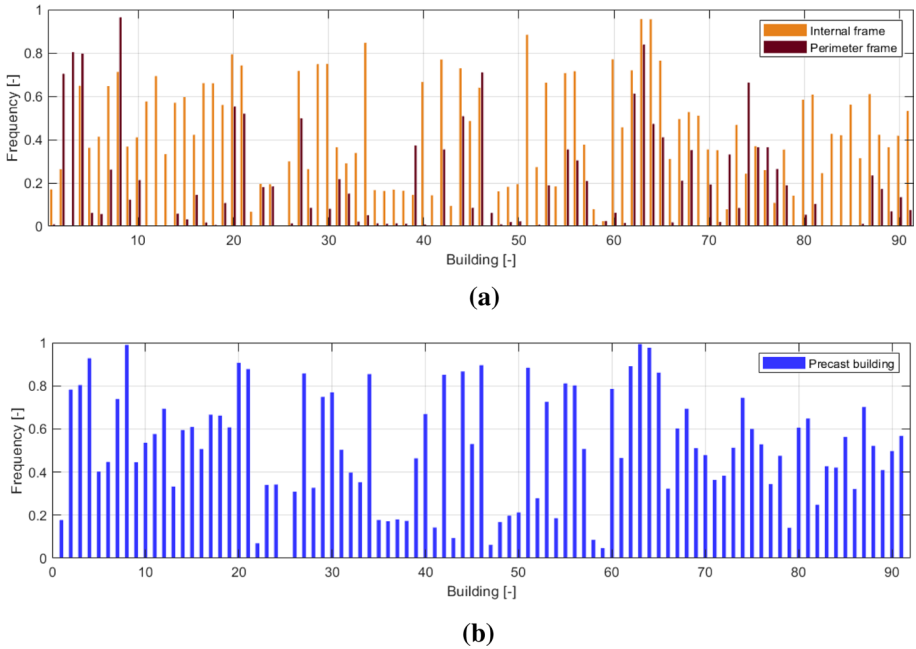|	Average orientation 70° $N_{c,est}$ (−)	Average orientation 160° $N_{c,est}$ (−)
SIN1	26.4	30.9
SIN2	21.5	25.2
SIN3	24.5	22.4

(a)

(b)

Fig. 12 Disaggregation of the outcomes for the seismic input SIN3. The histograms represent the number of collapse cases out of the 100,000 simulations for the 91 buildings, with reference to: **a** internal frames (in orange) and perimeter frames (in red), and **b** whole precast buildings (in blue)

Once the P_B of all the buildings in the industrial cluster are estimated, the assessment of the number of collapsed buildings over the entire stock can be directly derived through a statistical combination. Considering that each precast building in the case-study stock has the same probability (equal to 1/91) to be randomly extracted from the population (the building stock), the combined average collapse probability of the mixed set of buildings considered (named P_{eq}) is computed with following the procedure outlined in Shinozuka et al. (2000):

$$P_{eq} = \sum_{i=1}^{N} P_{B,i} \cdot \frac{n_i}{N} = \sum_{i=1}^{N} P_{B,i} \cdot \frac{1}{N} = \frac{1}{N} \sum_{i=1}^{N} P_{B,i} \tag{8}$$

where: n_i is the cardinality of the i-th precast building equal to 1; N is the total number of buildings in the stock, equal to 91; $P_{B,i}$ is the probability of collapse of the i-th building. Since P_{eq} can be also computed with the following ratio:

$$P_{eq} = N_{c,est}/N \tag{9}$$

where $N_{c,est}$ is the number of collapsed buildings estimated. By comparing Eqs. (8) and (9), the following expression can be derived:

$$N_{c,est} = \sum_{i=1}^{N} P_{B,i} \tag{10}$$

Under these hypotheses, the DS calculation allows a direct assessment of the expected number of precast buildings exceeding a specific limit state (the collapse in the present
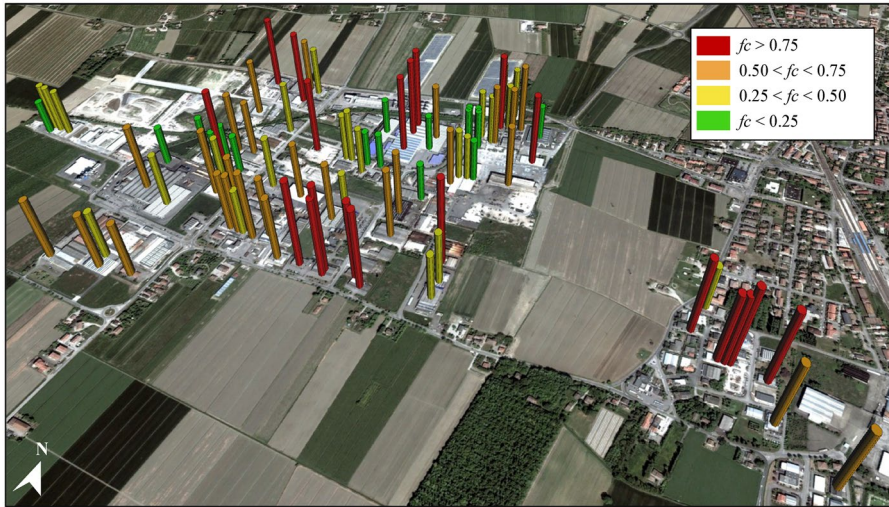
Fig. 13 Google Earth (2021) aerial view of the case-study area with histograms representing the frequency of occurrence of the collapse condition (fc) of the Monte Carlo simulations, for each of the 91 buildings; disaggregation of the Monte Carlo results (seismic input SIN3)

Table 5 Outcomes of the direct simplified (DS) calculation for the three seismic input: $N_{c,est}$ is the estimated number of collapsed buildings in the stock; P_{eq} is the combined average collapse probability; E_R is the relative error in percentage

	$N_{c,est}$ (−)	P_{eq} (%)	E_R (%)
SIN1	56.4	61.9	+ 34.3
SIN2	46.2	50.7	+ 10.0
SIN3	46.2	50.8	+ 10.1

case) in the building stock or in the productive area of interest. This straightforward calculation was carried out for the three seismic input models described in Sect. 4.1.

The results are reported in Table 5. The prediction error was computed with respect to the actual number of collapsed buildings ($N_{c,act} = 42$). The seismic inputs SIN2 and SIN3 are again deemed suitable for estimating the number of collapsed buildings in the case-study area, since the results differ about 10% with respect to the in-field real number of collapses observed after the 2012 earthquake. The outcomes of the DS procedure are in very good agreement with the mean value of collapsed buildings computed via MC simulations (see Table 2), for the three seismic inputs. Of course, the simplified method does not allow to estimate the uncertainty in the prediction, which is a peculiarity of MC method. The results suggest that this simplified but rapid procedure can be adopted as possible alternative to the MC simulation for large-scale applications.

5 Concluding remarks

A large-scale seismic damage assessment was performed to estimate the number of a set of precast RC buildings, located in the productive area of San Felice sul Panaro (Modena), collapsed during the 2012 seismic events. The scenario prediction of the seismic event of

the 29th May 2012 was outlined considering three different seismic input models, and comparing the results with the actual number of collapses occurred. The fragility curves of the precast frames obtained with the PRESSAFE-disp method have been adopted to perform a large-scale Monte Carlo simulation and, as an alternative, a direct simplified calculation.

In terms of number of collapsed buildings, the agreement with the actual effects of the earthquake is very good with both methods, in particular for the seismic input which takes the ground-motion directionality into account, usually not considered in the calculations of damage scenarios.

The results show a small overestimation of the number of collapsed buildings for all the three seismic input models. This discrepancy is, in part, due to the simplified modelling assumptions, related to the lack of precise structural knowledge of the geometries and the material properties of the buildings, a typical condition when the analyses are conducted at the territorial level. In the literature, several studies focusing on the seismic response evaluation of individual precast buildings exist, but the level of details required is usually not compatible with that of a large-scale structural assessment. Instead, the procedure proposed in this study requires few data, mainly available from a visual building survey, and suitable for a large-scale assessment in which many uncertainties on the structural behaviour are present.

It is worth noting that, to acquire rapid results, the direct simplified calculation constitutes a valid alternative to the Monte Carlo simulation, which is more computationally expensive and complex. However, the MC simulation allows to take the uncertainties of the problem into account, and to disaggregate the results, offering a more detailed analysis of the predictions.

Furthermore, the outcomes presented in this study suggest that the collapse fragility curves of the PRESSAFE-disp method can be reliably adopted for large-scale seismic assessment of precast RC buildings. Nonetheless, future developments can provide additional confirmations of the applicability of the procedure and suggest possible improvements. In particular, the scenario assessments of other case-studies could be conducted, considering also different damage conditions of the precast RC buildings included in the library of the fragility curves of the PRESSAFE-disp method.

This method represents a first attempt to set a uniform approach in the development of fragility curves of precast RC buildings to be used in large-scale evaluations. The availability of a general method allowing to study a diversified portfolio of precast buildings could be extremely useful to perform seismic scenario assessments aimed at the evaluation of the seismic losses. Future applications could address the definition of a unique method for the large-scale damage and loss evaluation of precast RC buildings. By defining the expected number of buildings reaching different damage levels, the additional computation of the seismic economic losses could be conducted to evaluate the financial consequences of the ground-motion in a performance-based approach. In this context, the large-scale application of this method gives valuable information for decision-making processes, aimed at identifying the prioritization of the seismic retrofitting of precast RC buildings, for example in Civil Protection or Government plans. This will be the object of future works and investigations.

Appendix

See Tables 6 and 7.

Table 6 PRESSAFE-disp coefficients (a1-b4) for the 91 internal frame fragility curves in San Felice; median value (μC) and standard deviation (σC) at the collapse limit state

# building	μ^C (I)	σ^C (I)	a1	a2	a3	b1	b2	b3	b4
1	0.320	0.549	0.070	−0.358	0.624	0.086	−0.491	0.675	0.284
2	0.342	0.493	0.070	−0.306	0.564	0.078	−0.462	0.589	0.281
3	0.000	0.000	0.000	0.000	0.000	0.000	0.000	0.000	0.000
4	0.385	0.494	0.070	−0.306	0.564	0.078	−0.462	0.589	0.281
5	0.183	0.461	0.050	−0.252	0.400	0.079	−0.430	0.565	0.255
6	0.478	0.495	0.070	−0.358	0.624	0.086	−0.491	0.675	0.284
7	0.344	0.427	0.053	−0.237	0.440	0.073	−0.426	0.542	0.263
8	0.256	0.463	0.047	−0.265	0.440	0.076	−0.400	0.559	0.232
9	0.216	0.467	0.047	−0.265	0.440	0.076	−0.400	0.559	0.232
10	0.180	0.267	0.053	−0.237	0.440	0.073	−0.426	0.542	0.263
11	0.179	0.431	0.067	−0.325	0.513	0.084	−0.467	0.614	0.273
12	0.169	0.414	0.067	−0.325	0.513	0.084	−0.467	0.614	0.273
13	0.165	0.405	0.067	−0.325	0.513	0.084	−0.467	0.614	0.273
14	0.297	0.508	0.067	−0.325	0.513	0.084	−0.467	0.614	0.273
15	0.405	0.486	0.070	−0.306	0.564	0.078	−0.462	0.589	0.281
16	0.361	0.497	0.070	−0.306	0.564	0.078	−0.462	0.589	0.281
17	0.341	0.447	0.069	−0.322	0.523	0.084	−0.504	0.589	0.254
18	0.361	0.479	0.067	−0.325	0.513	0.084	−0.467	0.614	0.273
19	0.285	0.509	0.067	−0.325	0.513	0.084	−0.467	0.614	0.273
20	0.383	0.460	0.067	−0.325	0.513	0.084	−0.467	0.614	0.273
21	0.409	0.438	0.072	−0.359	0.560	0.059	−0.316	0.385	0.322
22	0.253	0.352	0.070	−0.306	0.564	0.078	−0.462	0.589	0.281
23	0.328	0.552	0.070	−0.358	0.624	0.086	−0.491	0.675	0.284
24	0.328	0.552	0.070	−0.358	0.624	0.086	−0.491	0.675	0.284
25	0.000	0.000	0.000	0.000	0.000	0.000	0.000	0.000	0.000
26	0.209	0.415	0.070	−0.358	0.624	0.086	−0.491	0.675	0.284
27	0.436	0.529	0.070	−0.358	0.624	0.086	−0.491	0.675	0.284
28	0.205	0.467	0.067	−0.325	0.513	0.084	−0.467	0.614	0.273
29	0.164	0.402	0.067	−0.325	0.513	0.084	−0.467	0.614	0.273
30	0.138	0.408	0.050	−0.252	0.400	0.079	−0.430	0.565	0.255
31	0.163	0.444	0.050	−0.252	0.400	0.079	−0.430	0.565	0.255
32	0.240	0.497	0.067	−0.325	0.513	0.084	−0.467	0.614	0.273
33	0.220	0.483	0.067	−0.325	0.513	0.084	−0.467	0.614	0.273
34	0.278	0.448	0.050	−0.252	0.400	0.079	−0.430	0.565	0.255
35	0.228	0.489	0.067	−0.325	0.513	0.084	−0.467	0.614	0.273
36	0.225	0.487	0.067	−0.325	0.513	0.084	−0.467	0.614	0.273
37	0.228	0.489	0.067	−0.325	0.513	0.084	−0.467	0.614	0.273
38	0.225	0.487	0.067	−0.325	0.513	0.084	−0.467	0.614	0.273
39	0.322	0.550	0.070	−0.358	0.624	0.086	−0.491	0.675	0.284
40	0.368	0.473	0.067	−0.325	0.513	0.084	−0.467	0.614	0.273
41	0.297	0.537	0.070	−0.358	0.624	0.086	−0.491	0.675	0.284
42	0.244	0.469	0.050	−0.252	0.400	0.079	−0.430	0.565	0.255
43	0.271	0.460	0.092	−0.467	0.735	0.085	−0.447	0.553	0.321
44	0.225	0.473	0.050	−0.252	0.400	0.079	−0.430	0.565	0.255
45	0.199	0.371	0.092	−0.467	0.735	0.085	−0.447	0.553	0.321

Table 6 (continued)

# building	μ^C (I)	σ^C (I)	a1	a2	a3	b1	b2	b3	b4
46	0.216	0.473	0.050	−0.252	0.400	0.079	−0.430	0.565	0.255
47	0.000	0.000	0.000	0.000	0.000	0.000	0.000	0.000	0.000
48	0.224	0.486	0.067	−0.325	0.513	0.084	−0.467	0.614	0.273
49	0.239	0.497	0.067	−0.325	0.513	0.084	−0.467	0.614	0.273
50	0.242	0.498	0.067	−0.325	0.513	0.084	−0.467	0.614	0.273
51	0.138	0.331	0.067	−0.325	0.513	0.084	−0.467	0.614	0.273
52	0.234	0.494	0.067	−0.325	0.513	0.084	−0.467	0.614	0.273
53	0.336	0.495	0.067	−0.325	0.513	0.084	−0.467	0.614	0.273
54	0.197	0.459	0.067	−0.325	0.513	0.084	−0.467	0.614	0.273
55	0.223	0.473	0.050	−0.252	0.400	0.079	−0.430	0.565	0.255
56	0.448	0.521	0.070	−0.358	0.624	0.086	−0.491	0.675	0.284
57	0.270	0.508	0.067	−0.325	0.513	0.084	−0.467	0.614	0.273
58	0.234	0.376	0.069	−0.322	0.523	0.084	−0.504	0.589	0.254
59	0.360	0.456	0.088	−0.434	0.809	0.081	−0.425	0.531	0.337
60	0.255	0.464	0.050	−0.252	0.400	0.079	−0.430	0.565	0.255
61	0.291	0.509	0.067	−0.325	0.513	0.084	−0.467	0.614	0.273
62	0.347	0.359	0.050	−0.252	0.400	0.079	−0.430	0.565	0.255
63	0.273	0.452	0.050	−0.252	0.400	0.079	−0.430	0.565	0.255
64	0.271	0.453	0.050	−0.252	0.400	0.079	−0.430	0.565	0.255
65	0.282	0.444	0.050	−0.252	0.400	0.079	−0.430	0.565	0.255
66	0.377	0.555	0.070	−0.358	0.624	0.086	−0.491	0.675	0.284
67	0.420	0.539	0.070	−0.358	0.624	0.086	−0.491	0.675	0.284
68	0.283	0.509	0.067	−0.325	0.513	0.084	−0.467	0.614	0.273
69	0.184	0.440	0.067	−0.325	0.513	0.084	−0.467	0.614	0.273
70	0.250	0.502	0.067	−0.325	0.513	0.084	−0.467	0.614	0.273
71	0.249	0.501	0.067	−0.325	0.513	0.084	−0.467	0.614	0.273
72	0.451	0.521	0.088	−0.434	0.809	0.081	−0.425	0.531	0.337
73	0.195	0.563	0.050	−0.249	0.408	0.087	−0.387	0.582	0.275
74	0.243	0.499	0.067	−0.325	0.513	0.084	−0.467	0.614	0.273
75	0.265	0.507	0.067	−0.325	0.513	0.084	−0.467	0.614	0.273
76	0.517	0.532	0.088	−0.434	0.809	0.081	−0.425	0.531	0.337
77	0.213	0.393	0.053	−0.237	0.440	0.073	−0.426	0.542	0.263
78	0.158	0.438	0.050	−0.252	0.400	0.079	−0.430	0.565	0.255
79	0.192	0.451	0.067	−0.325	0.513	0.084	−0.467	0.614	0.273
80	0.208	0.472	0.050	−0.252	0.400	0.079	−0.430	0.565	0.255
81	0.166	0.446	0.067	−0.339	0.527	0.113	−0.610	0.780	0.274
82	0.201	0.463	0.067	−0.325	0.513	0.084	−0.467	0.614	0.273
83	0.157	0.387	0.067	−0.325	0.513	0.084	−0.467	0.614	0.273
84	0.388	0.455	0.067	−0.325	0.513	0.084	−0.467	0.614	0.273
85	0.369	0.472	0.067	−0.325	0.513	0.084	−0.467	0.614	0.273
86	0.241	0.498	0.067	−0.325	0.513	0.084	−0.467	0.614	0.273
87	0.313	0.504	0.067	−0.325	0.513	0.084	−0.467	0.614	0.273
88	0.415	0.542	0.070	−0.358	0.624	0.086	−0.491	0.675	0.284
89	0.472	0.501	0.070	−0.358	0.624	0.086	−0.491	0.675	0.284
90	0.537	0.426	0.070	−0.358	0.624	0.086	−0.491	0.675	0.284
91	0.469	0.411	0.063	−0.383	0.563	0.083	−0.479	0.547	0.301

Table 7 PRESSAFE-disp coefficients (a1–b4) for the 91 perimeter frame fragility curves in San Felice; median value (μC) and standard deviation (σC) at the collapse limit state

# building	μ^C (P)	σ^C (P)	a1	a2	a3	b1	b2	b3	b4
1	1.245	0.548	0.012	0.093	1.167	0.119	−0.525	0.546	0.384
2	0.429	0.368	0.095	−0.426	0.667	0.132	−0.645	0.689	0.156
3	0.452	0.364	0.095	−0.426	0.667	0.132	−0.645	0.689	0.156
4	0.478	0.355	0.095	−0.426	0.667	0.132	−0.645	0.689	0.156
5	0.783	0.442	0.011	−0.004	0.779	0.043	−0.160	0.090	0.449
6	0.773	0.529	0.120	−0.510	0.922	0.135	−0.664	0.788	0.342
7	0.536	0.807	0.083	−0.354	0.640	0.130	−0.495	0.422	0.719
8	0.303	0.376	0.069	−0.347	0.480	0.069	−0.385	0.397	0.262
9	0.727	0.455	0.011	−0.004	0.724	0.039	−0.150	0.097	0.449
10	0.270	0.630	0.083	−0.354	0.640	0.130	−0.495	0.422	0.719
11	1.086	0.491	0.034	−0.044	1.095	0.087	−0.411	0.527	0.290
12	1.088	0.488	0.034	−0.044	1.095	0.087	−0.411	0.527	0.290
13	1.089	0.486	0.034	−0.044	1.095	0.087	−0.411	0.527	0.290
14	1.081	0.472	0.034	−0.044	1.095	0.087	−0.411	0.527	0.290
15	1.005	0.469	0.033	−0.045	1.018	0.079	−0.386	0.569	0.290
16	1.003	0.506	0.033	−0.045	1.018	0.079	−0.386	0.569	0.290
17	1.217	0.504	0.033	−0.041	1.229	0.086	−0.351	0.521	0.329
18	1.083	0.433	0.034	−0.044	1.095	0.087	−0.411	0.527	0.290
19	1.081	0.477	0.034	−0.044	1.095	0.087	−0.411	0.527	0.290
20	0.494	0.332	0.091	−0.435	0.620	0.120	−0.606	0.744	0.156
21	0.564	0.382	0.077	−0.420	0.693	0.124	−0.617	0.729	0.205
22	1.010	0.554	0.033	−0.045	1.018	0.079	−0.386	0.569	0.290
23	0.613	0.616	0.120	−0.510	0.922	0.135	−0.664	0.788	0.342
24	0.613	0.616	0.120	−0.510	0.922	0.135	−0.664	0.788	0.342
25	1.264	0.533	0.012	0.093	1.167	0.119	−0.525	0.546	0.384
26	0.470	0.551	0.120	−0.510	0.922	0.135	−0.664	0.788	0.342
27	0.565	0.406	0.099	−0.470	0.744	0.115	−0.571	0.713	0.200
28	0.658	0.688	0.097	−0.393	0.936	0.149	−0.631	0.482	0.661
29	1.089	0.486	0.034	−0.044	1.095	0.087	−0.411	0.527	0.290
30	0.451	0.672	0.083	−0.337	0.711	0.127	−0.550	0.440	0.666
31	0.478	0.713	0.083	−0.337	0.711	0.127	−0.550	0.440	0.666
32	0.693	0.728	0.097	−0.393	0.936	0.149	−0.631	0.482	0.661
33	1.082	0.494	0.034	−0.044	1.095	0.087	−0.411	0.527	0.290
34	0.779	0.462	0.011	−0.004	0.779	0.043	−0.160	0.090	0.449
35	1.082	0.494	0.034	−0.044	1.095	0.087	−0.411	0.527	0.290
36	1.082	0.494	0.034	−0.044	1.095	0.087	−0.411	0.527	0.290
37	1.082	0.494	0.034	−0.044	1.095	0.087	−0.411	0.527	0.290
38	1.082	0.494	0.034	−0.044	1.095	0.087	−0.411	0.527	0.290
39	0.446	0.462	0.099	−0.470	0.744	0.115	−0.571	0.713	0.200
40	1.084	0.428	0.034	−0.044	1.095	0.087	−0.411	0.527	0.290
41	0.000	0.000	0.000	0.000	0.000	0.000	0.000	0.000	0.000
42	0.560	0.764	0.083	−0.337	0.711	0.127	−0.550	0.440	0.666
43	0.000	0.000	0.000	0.000	0.000	0.000	0.000	0.000	0.000
44	0.541	0.760	0.083	−0.337	0.711	0.127	−0.550	0.440	0.666
45	0.362	0.466	0.138	−0.653	0.960	0.115	−0.576	0.714	0.247

Table 7 (continued)

# building	μ^C (P)	σ^C (P)	a1	a2	a3	b1	b2	b3	b4
46	0.301	0.471	0.071	− 0.341	0.487	0.130	− 0.643	0.764	0.213
47	0.426	0.547	0.121	− 0.544	0.907	0.131	− 0.650	0.838	0.252
48	1.082	0.494	0.034	− 0.044	1.095	0.087	− 0.411	0.527	0.290
49	1.081	0.492	0.034	− 0.044	1.095	0.087	− 0.411	0.527	0.290
50	1.081	0.491	0.034	− 0.044	1.095	0.087	− 0.411	0.527	0.290
51	1.097	0.468	0.034	− 0.044	1.095	0.087	− 0.411	0.527	0.290
52	1.081	0.493	0.034	− 0.044	1.095	0.087	− 0.411	0.527	0.290
53	0.782	0.764	0.097	− 0.393	0.936	0.149	− 0.631	0.482	0.661
54	1.084	0.494	0.034	− 0.044	1.095	0.087	− 0.411	0.527	0.290
55	0.519	0.750	0.083	− 0.337	0.711	0.127	− 0.550	0.440	0.666
56	0.741	0.556	0.120	− 0.510	0.922	0.135	− 0.664	0.788	0.342
57	0.721	0.748	0.097	− 0.393	0.936	0.149	− 0.631	0.482	0.661
58	1.218	0.572	0.033	− 0.041	1.229	0.086	− 0.351	0.521	0.329
59	0.567	0.504	0.132	− 0.607	1.056	0.110	− 0.547	0.685	0.259
60	0.780	0.460	0.011	− 0.004	0.779	0.043	− 0.160	0.090	0.449
61	1.081	0.477	0.034	− 0.044	1.095	0.087	− 0.411	0.527	0.290
62	0.436	0.317	0.071	− 0.341	0.487	0.130	− 0.643	0.764	0.213
63	0.361	0.425	0.071	− 0.341	0.487	0.130	− 0.643	0.764	0.213
64	0.587	0.763	0.083	− 0.337	0.711	0.127	− 0.550	0.440	0.666
65	0.371	0.414	0.071	− 0.341	0.487	0.130	− 0.643	0.764	0.213
66	1.225	0.547	0.012	0.093	1.167	0.119	− 0.525	0.546	0.384
67	0.712	0.577	0.120	− 0.510	0.922	0.135	− 0.664	0.788	0.342
68	0.733	0.754	0.097	− 0.393	0.936	0.149	− 0.631	0.482	0.661
69	1.085	0.492	0.034	− 0.044	1.095	0.087	− 0.411	0.527	0.290
70	0.702	0.735	0.097	− 0.393	0.936	0.149	− 0.631	0.482	0.661
71	1.081	0.489	0.034	− 0.044	1.095	0.087	− 0.411	0.527	0.290
72	0.531	0.614	0.116	− 0.522	0.853	0.126	− 0.631	0.922	0.227
73	0.775	0.426	0.011	− 0.004	0.771	0.040	− 0.176	0.082	0.449
74	0.344	0.424	0.091	− 0.435	0.620	0.120	− 0.606	0.744	0.156
75	0.318	0.424	0.091	− 0.435	0.620	0.120	− 0.606	0.744	0.156
76	0.754	0.492	0.132	− 0.607	1.056	0.110	− 0.547	0.685	0.259
77	0.377	0.783	0.083	− 0.354	0.640	0.130	− 0.495	0.422	0.719
78	0.473	0.706	0.083	− 0.337	0.711	0.127	− 0.550	0.440	0.666
79	1.084	0.494	0.034	− 0.044	1.095	0.087	− 0.411	0.527	0.290
80	0.781	0.451	0.011	− 0.004	0.779	0.043	− 0.160	0.090	0.449
81	0.381	0.596	0.129	− 0.566	0.841	0.133	− 0.637	0.745	0.367
82	1.084	0.495	0.034	− 0.044	1.095	0.087	− 0.411	0.527	0.290
83	1.091	0.482	0.034	− 0.044	1.095	0.087	− 0.411	0.527	0.290
84	0.000	0.000	0.000	0.000	0.000	0.000	0.000	0.000	0.000
85	1.084	0.428	0.034	− 0.044	1.095	0.087	− 0.411	0.527	0.290
86	1.081	0.491	0.034	− 0.044	1.095	0.087	− 0.411	0.527	0.290
87	0.761	0.762	0.097	− 0.393	0.936	0.149	− 0.631	0.482	0.661
88	0.707	0.581	0.120	− 0.510	0.922	0.135	− 0.664	0.788	0.342
89	0.767	0.535	0.120	− 0.510	0.922	0.135	− 0.664	0.788	0.342
90	0.662	0.311	0.099	− 0.470	0.744	0.115	− 0.571	0.713	0.200
91	0.742	0.312	0.104	− 0.442	0.818	0.107	− 0.565	0.684	0.206

Declarations

References

Agenzia regionale per la Ricostruzione – Sisma 2012. (2018) Analisi tecnico-economica della ricostruzione post sisma degli edifici produttivi. Centro Stampa Regione Emilia-Romagna, Bologna. (in Italian). https://www.regione.emilia-romagna.it/terremoto

Anglade E, Giatreli AM, Blyth A et al (2020) Seismic damage scenarios for the Historic City Center of Leiria, Portugal: analysis of the impact of different seismic retrofitting strategies on emergency planning. Int J Disast Risk Re 44:101432. https://doi.org/10.1016/j.ijdrr.2019.101432

Asteris PG, Antoniou ST, Sophianopoulos DS, Chrysostomou CZ (2011) Mathematical macromodeling of infilled frames: state of the art. ASCE J Struct Eng 137(12):1508–1517. https://doi.org/10.1061/(ASCE)ST.1943-541X.0000384

Babič A, Dolšek M (2016) Seismic fragility functions of industrial precast building classes. Eng Struct 118:357–370. https://doi.org/10.1016/j.engstruct.2016.03.069

Batalha N, Rodrigues H, Varum H (2019) Seismic performance of RC precast industrial buildings— learning with the past earthquakes. Innov Infrastruct Solut 4(4):1–13. https://doi.org/10.1007/s41062-018-0191-y

Belleri A, Brunesi E, Nascimbene R, Pagani M, Riva P (2014) Seismic performance of precast industrial facilities following major earthquakes in the Italian territory. J Perform Constr Facil 29(5):04014135. https://doi.org/10.1061/(ASCE)CF.1943-5509.0000617

Belleri A, Torquati M, Riva P, Nascimbene R (2015) Vulnerability assessment and retrofit solutions of precast industrial structures. Earthq Struct 8(3):801–820

Belleri A, Torquati M, Marini A, Riva P (2016) Horizontal cladding panels: in-plane seismic performance in precast concrete buildings. Bull Earthq Eng 14:1103–1129. https://doi.org/10.1007/s10518-015-9861-8

Belleri A, Labò S, Marini A, Riva P (2017) The Influence of overhead cranes in the seismic performance of industrial buildings. Front Built Environ 3:64. https://doi.org/10.3389/fbuil.2017.00064

Belleri A, Cornali F, Passoni C, Marini A, Riva P (2018) Evaluation of out-of-plane seismic performance of column-to-column precast concrete cladding panels in one-storey industrial buildings. Earthq Eng Struct Dyn 47:397–417. https://doi.org/10.1002/eqe.2956

Belleri A, Dal Lago B, Rodrigues H (2021) Editorial: advances in seismic performance and risk estimation of precast concrete buildings. Front Built Environ 7:822262. https://doi.org/10.3389/fbuil.2021.822262

Bellotti D, Casotto C, Crowley H, Deyanova MG, Germagnoli F, Fianchisti G, Lucarelli E, Riva S, Nascimbene R (2014) Single-storey precast buildings: probabilistic distribution of structural systems and subsystems from the sixties. Prog Sismica 5(3):41–70 (**in Italian**))

Benjamin JR, Cornell CA (1970) Probability, statistics, and decision for civil engineers. McGraw-Hill Book Company, United States of America

Biondini F, Dal Lago B, Toniolo G (2013) Role of wall panel connections on the seismic performance of precast structures. Bull Earthq Eng 11:1061–1081

Bonfanti C, Carabellese A, Toniolo G. (2008) Strutture prefabbricate: catalogo delle tipologie esistenti. Assobeton. (in Italian). http://www.reluis.it/

Bosio M, Belleri A, Riva P, Marini A (2020) Displacement-based simplified seismic loss assessment of Italian precast buildings. J Earthq Eng 24(1):60–81. https://doi.org/10.1080/13632469.2020.1724215

Bournas DA, Negro P, Molina FJ (2013) Pseudodynamic tests on a full-scale 3-storey precast concrete building: behavior of the mechanical connections and floor diaphragms. Eng Struct 57:609–627

Bournas DA, Negro P, Taucer F (2014) Performance of industrial buildings during the Emilia earthquakes in Northern Italy and recommendations for their strengthening. Bull Earthq Eng 12:2383–2404. https://doi.org/10.1007/s10518-013-9466-z

Bovo M, Savoia M (2018) Numerical simulation of seismic-induced failure of a precast structure during the Emilia earthquake. J Perform Constr Facil 32(1):04017119. https://doi.org/10.1061/(ASCE)CF.1943-5509.0001086

Bovo M, Savoia M (2019) Evaluation of force fluctuations induced by vertical seismic component on reinforced concrete precast structures. Eng Struct 179:70–87. https://doi.org/10.1016/j.engstruct.2018.10.018

Bovo M, Savoia M (2021) Fast seismic assessment of existing precast structures by means of fragility surfaces: the PRESSAFE methodology. J Earthq Eng. https://doi.org/10.1080/13632469.2021.1964648

Bovo M, Praticò L, Savoia M (2022) PRESSAFE-disp: an alternative method for the fast in-plane seismic assessment of existing precast RC buildings after the Emilia earthquake of May 2012. Bull Earthq Eng 20:2751–2794. https://doi.org/10.1007/s10518-022-01318-x

Brunesi E, Nascimbene R, Peloso S (2020) Evaluation of the seismic response of precast wall connections: experimental observations and numerical modelling. J Earthq Eng 24(7):1057–1082. https://doi.org/10.1080/13632469.2018.1469440

Buratti N, Minghini F, Ongaretto E, Savoia M, Tullini N (2017) Empirical seismic fragility for the precast RC industrial buildings damaged by the 2012 Emilia (Italy) earthquakes. Earthq Eng Struct Dyn 46(14):2317–2335. https://doi.org/10.1002/eqe.2906

Calvi GM, Pinho R, Magenes G, Bommer JJ, Restrepo-Vélez LF, Crowley H (2006) Development of seismic vulnerability assessment methodologies over the past 30 years. ISET J Earthq Technol 43(3):75–104

Casotto C, Silva V, Crowley H, Nascimbene R, Pinho R (2015) Seismic fragility of Italian RC precast industrial structures. Eng Struct 94:122–136

Crisafulli FJ, Carr AJ, Park R (2000) Analytical modelling of infilled frame structures - a general review. Bull NZ Soc Earthq Eng 33(1):30–47. https://doi.org/10.5459/bnzsee.33.1.30-47

da Porto F, Donà M, Rosti A et al (2021) Comparative analysis of the fragility curves for Italian residential masonry and RC buildings. Bull Earthq Eng 19:3209–3252. https://doi.org/10.1007/s10518-021-01120-1

Dal Lago B, Ferrara L (2018) Efficacy of roof-to-beam mechanical connections on the diaphragm behaviour of precast decks with spaced roof elements. Eng Struct 176:681–696. https://doi.org/10.1016/j.engstruct.2018.09.027

Dal Lago B, Bianchi S, Biondini F (2019) Diaphragm effectiveness of precast concrete structures with cladding panels under seismic action. Bull Earthq Eng 17(1):473–495. https://doi.org/10.1007/s10518-018-0452-3

Del Monte E, Falsini C, Boschi S, Menichini G, Orlando M (2019) An innovative cladding panel connection for RC precast buildings. Bull Earthq Eng 17:845–865. https://doi.org/10.1007/s10518-018-0470-1

Demartino C, Vanzi I, Monti G (2017) Probabilistic estimation of seismic economic losses of portal-like precast industrial buildings. Earthq Struct 13(3):323–335

Dolce M, Nicoletti M, Ammirati A. et al. (2012) The Ferrara arc thrust earthquakes of May-June 2012 (Northern Italy): strong-motion and geological observations. Mirandola Earthquake Working Group - Report 2. http://www.protezionecivile.gov.it/

Google Earth. Accessed 13 Dec 2022. https://www.google.it/intl/it/earth/

Ercolino M, Bellotti D, Magiulo G, Nascimbene R (2018a) Vulnerability analysis of industrial RC precast buildings designed according to modern seismic codes. Eng Struct 158:67–78. https://doi.org/10.1016/j.engstruct.2017.12.005

Ercolino M, Petrone C, Magliulo G, Manfredi G (2018b) Seismic Design of single-story precast structures for P-Δ effects. ACI Struct J 115(4):943–955. https://doi.org/10.14359/51701915

FEMA - Federal Emergency Management Agency (2018) FEMA P-58–1: Seismic performance assessment of buildings: volume 1 – methodology. Second Edition. Washington, DC

Fisz M (1963) Probability theory and mathematical statistics. Wiley, New York

Formisano A, Chieffo N, Mosoarca M. (2017) Probabilistic damage scenario: a case study in Amatrice affected by the 2016 seismic sequence. In: Proceedings of 3rd international conference PROHITECH, Lisbon

Grigoriu M (2002) Stochastic calculus – applications in science and engineering. Birkhäuser, Boston, MA. https://doi.org/10.1007/978-0-8176-8228-6

Itaca database. Accessed 13 Dec 2022. http://itaca.mi.ingv.it/ItacaNet_31/#/home

Lestuzzi P, Podestà S, Luchini C et al (2016) Seismic vulnerability assessment at urban scale for two typical Swiss cities using Risk-UE methodology. Nat Hazards 84:249–269

Liberatore L, Sorrentino L, Liberatore D, Decanini LD (2013) Failure of industrial structures induced by the Emilia (Italy) 2012 earthquakes. Eng Fail Anal 34:629–647. https://doi.org/10.1016/j.engfailanal.2013.02.009

Magliulo G, Ercolino M, Petrone C, Coppola O, Manfredi G (2014) The Emilia earthquake: seismic performance of precast reinforced concrete buildings. Earthq Spectra 30(2):891–912. https://doi.org/10.1193/091012EQS285M

Magliulo G, Ercolino M, Cimmino M, Capozzi V, Manfredi G (2015) Cyclic shear test on a dowel beam-to-column connection of precast buildings. Earthq Struct 9(3):541–562

Magliulo G, Bellotti D, Cimmino M, Nascimbene R (2018) Modeling and seismic response analysis of RC precast Italian code-conforming buildings. J Earthq Eng 22(2):140–167. https://doi.org/10.1080/13632469.2018.1531093

Maio R, Ferreira TM, Vicente R, Estevao J (2015) Seismic vulnerability assessment of historical urban centres: case study of the old city centre of Faro. Portugal J Risk Res 19(5):551–580. https://doi.org/10.1080/13669877.2014.988285

Mandelli Contegni M, Palermo A, Toniolo G. (2007) Strutture prefabbricate: schedario dei collegamenti. Assobeton. (in Italian). http://www.reluis.it/

Mandelli Contegni M, Palermo A, Toniolo G. (2008) Strutture prefabbricate: schedario di edifici prefabbricati in C.A. Assobeton. (in Italian). http://www.reluis.it/

MathWorks. Accessed 10 June 2020. https://www.mathworks.com/products/matlab.html

Minghini F, Ongaretto E, Ligabue V, Savoia M, Tullini N (2016) Observational failure analysis of precast buildings after the 2012 Emilia earthquakes. Earthq Struct 11(2):327–346

Nastri E, Vergato M, Latour M (2017) Performance evaluation of a seismic retrofitted RC precast industrial building. Earthq Struct 12(1):13–21

Ongaretto E, Buratti N, Savoia M. (2019) Empirical seismic fragility of different typologies of precast RC industrial buildings. In: Proceedings of XVIII convegno anidis, Ascoli Piceno, Italy

Petruzzelli F (2016) Seismic risk assessment of an industrial plant struck by the Emilia 2012 earthquakes. Int J Forensic Eng 3(1–2):146–163

Polese M, Di Ludovico M, Gaetani d'Aragona M, Prota A, Manfredi G (2020) Regional vulnerability and risk assessment accounting for local building typologies. Int J Disaster Risk Reduct 43:101400

Ramirez CM, Miranda E. (2009) Building-specific loss estimation methods & tools for simplified performance-based earthquake engineering. Report No.171. The John A. Blume Earthquake Engineering Center, Stanford

ReLUIS (2012) Linee di indirizzo per interventi locali e globali su edifici industriali monopiano non progettati con criteri antisismici. Gruppo di Lavoro Agibilità Sismica dei Capannoni Industriali. (in Italian). http://www.reluis.it/

Rodrigues D, Crowley H, Silva V (2018) Earthquake loss assessment of precast RC industrial structures in Tuscany (Italy). Bull Earthq Eng 16:203–228. https://doi.org/10.1007/s10518-017-0195-6

Rossi L, Stupazzini M, Parisi D, Holtschoppen B, Ruggieri G, Butenweg C (2020) Empirical fragility functions and loss curves for Italian business facilities based on the 2012 Emilia-Romagna earthquake official database. Bull Earthq Eng 18:1693–1721. https://doi.org/10.1007/s10518-019-00759-1

Rovida A, Locati M, Camassi R, Lolli B, Gasperini P (2020) The Italian earthquake catalogue CPTI15. Bull Earthq Eng 18(7):2953–2984. https://doi.org/10.1007/s10518-020-00818-y

Rovida A, Locati M, Camassi R, Lolli, B, Gasperini P, Antonucci A. (2022) Catalogo Parametrico dei Terremoti Italiani (CPTI15), versione 4.0. Istituto Nazionale di Geofisica e Vulcanologia (INGV). https://doi.org/10.13127/CPTI/CPTI15.4

Savoia M, Mazzotti C, Buratti N, Ferracuti B, Bovo M, Ligabue V, Vincenzi L (2012) Damages and collapses in industrial precast buildings after the Emilia earthquake. Ing Sismica 29(2):120–131

Savoia M, Buratti N, Vincenzi L (2017) Damage and collapse in industrial precast buildings after the 2012 Emilia earthquake. Eng Struct 137:162–180. https://doi.org/10.1016/j.engstruct.2017.01.059

Shinozuka M, Feng MQ, Kim H, Uzawa T, Ueda T (2000) Statistical analysis of fragility curves. J Eng Mech 126(12):1224–1231. https://doi.org/10.1061/(ASCE)0733-9399(2000)126:12(1224)

Silva V, Akkar S, Baker J, Bazzurro P, Castro JM, Crowley H, Dolsek M, Galasso C, Lagomarsino S, Monteiro R, Perrone D, Pitilakis K, Vamvatsikos D (2019) Current challenges and future trends in analytical fragility and vulnerability modelling. Earthq Spectra 35(4):1927–1952. https://doi.org/10.1193/042418EQS101O

Soydan C, Yuksel E, Irtem E (2020) Seismic performance improvement of single-storey precast reinforced concrete industrial buildings in use. Soil Dyn Earthq Eng 135:106167. https://doi.org/10.1016/j.soildyn.2020.106167

Vamvatsikos D, Fragiadakis M (2010) Incremental dynamic analysis for estimating seismic performance sensitivity and uncertainty. Earthq Eng Struct Dyn 39:141–163

Villar-Vega M, Silva V, Crowley H, Yepes C, Tarque N, Acevedo AB, Hube MA, Coronel GD, Santa MH (2017) Development of a fragility model for the residential building stock in South America. Earthq Spectra 33(2):581–604. https://doi.org/10.1193/010716EQS005M

Worden CB, Thompson EM, Baker JW, Bradley BA, Luco N, Wald DJ (2018) Spatial and spectral interpolation of ground motion intensity measure observations. Bull Seism Soc Am 108(2):866–875. https://doi.org/10.1785/0120170201

Zoubek B, Fischinger M, Isakovic T (2016) Cyclic response of hammer-head strap cladding-to-structure connections used in RC precast building. Eng Struct 119:135–148